Influence of cyclic sand ratcheting on monopile tilt accumulation

by

Himani Arya

to obtain the degree of Master of Science

at the Delft University of Technology,

Student number:	5161614	
Project duration:	June 15, 2021 – May 31, 2022	
Thesis committee:	Prof. dr. M. A. Hicks	TU Delft, committee chair
	Dr. Federico Pisano	TU Delft
	Dr. Ir. A. P. (Bram) van den Eijnden	TU Delft
	Zheng Li.	TU Delft

TU Delft

Acknowledgements

This master thesis includes guidance and expertise from many people, without whom it would have been really difficult to complete the objectives. I would like to express my sincere gratitude towards my chair supervisor Dr. Federico Pisano for introducing me to such interesting thesis topic and being really supportive and for encouraging feedback's throughout the thesis. I would like to thanks my daily supervisor Zheng Li for such close guidance and valuable advises through out my master thesis. I really enjoyed our weekly meetings giving me tips and drizzling me through your knowledge and experience in order to complete my thesis successfully. I am also grateful that my thesis got approval from all the committee members.

It was an honour to be a part of such highly reputated university Delft University of Technology (TU Delft), as a master's student which is famous world wide for its academic contributions. I joined TU Delft in 2019 and in my three years of masters, I not only grew and learned academically but also personally. I would like to appreciate here not only my professors who provided me with academic assistant but also my multi cultural classmates who made me feel welcomed and also helped me as an international student.

My special thanks will go to my family, sister (Bhawana Arya) and friends back home in India for being patient and supportive for my all decisions. I would also like to thank my small family in Netherlands Parth Sevlikar, Shaurya Verma and Saurab Nerker for being always available during my hard times. Finally, I would like to congratulate myself for surviving through one of the most challenging phase of my life with never giving up spirit.

Himani Arya
Delft,May 2022

Abstract

Limited natural resources and global warming have encouraged humanity to explore renewable sources such as offshore wind energy. Offshore wind structures are subjected to repeated environmental loads. These loads are quite complex in terms of frequencies and amplitudes, coming from different directions. To support these offshore wind turbines, monopiles are the most common foundations. The normal operation of a wind turbine requires limited rotation of foundations for fluctuating lateral loading. These fluctuating cyclic loads cause the accumulation of strains in the soil surrounding the foundation. However, current design originated from the oil and gas industry focuses on the vertical capacity of foundation and also underestimate the lateral stiffness of pile after cyclic loading. Hence, it becomes crucial to come up with a solution that takes account of cyclic soil- monopile interaction responses under lateral loading.

This thesis aims to bridge a gap between soil behaviour and monopile response to understand cyclic sand behavior and predict accumulated rotations/tilt in monopiles. A new soil constitutive model SANISAND-MS based on a bounding surface framework has been developed to replicate fabric-related processes and ratcheting behaviour by the evolution or contraction of the memory surface. Initially, the model has been calibrated against the experimental observations for the triaxial test as well as the DSS test under monotonic loading. Parameters that govern the cyclic ratcheting behaviour are investigated for 1000 cycles under the drained condition and results suggest that increasing memory surface parameter values, the secant stiffness increases which leads to less accumulated strain. Another set of analyses under a series of load parcels for loading sequence is done and superposition method is found to provide relevant accumulated strains when the load parcels are in ascending order.

3D Finite element modeling was set up to simulate monopile-soil interaction. Both soil and pile were discretized using solid elements, while the pile above the ground is built based on embedded beam elements. FE model can trace the effect of the memory surface parameters through accumulated rotations confirming that proposed model can reproduce experimental evidence regarding soil-monopile interaction. Empirical equations introduced to calculate accumulated rotations due to long-term loading compliments FE model for different pile geometry, and most dangerous situation (accumulated rotations) can be expected during two-way loading. The FEM also acknowledges influence of ratcheting properties by taking into account pile geometry response(length, diameter, thickness, and load eccentricity). Overall this thesis postulates, that FEM is a reliable model for replicating drained cyclic ratcheting behavior in sands and can further assist in the improvement of design methods.

Nomenclature

A_o = 'intrinsic' dilatancy Parameter

b^M = yield-to-memory surface distance

b_{ref} = reference distance for normalisation

b_o = hardening factor

C_u = uniformity coefficient

c = compression-to-extension strength ratio

c_h = hardening parameter

D = Dilatancy coefficient

e = void ratio

e= deviatoric strain tensor

e_c = void ratio at critical state

e_{in} = initial void ratio

e_o = reference critical void ratio

f = yield function

f^M = Memory function

f_{shr} = memory surface shrinkage geometrical factor

G = Shear Modulus

h = hardening factor

$\tilde{h}$ = virgin state hardening factor generalized into common situation

h^M = memory-counterpart of the hardening coefficient

h_0 = hardening parameter

I = second order Identity tensor

K_p = plastic modulus

L = plastic multiplier

L^M = Memory-counterpart of the plastic multiplier

M = critical stress ratio in compression

m = yield locus opening parameter

m^M = memory locus opening parameter

$N =$ no. of cycles

$N =$ unit tensor normal to the yield locus

$n^M =$ unit tensor for memory surface contraction

$n^{b,d} =$ void ratio dependence parameters

$p =$ mean effective stress

$p_{atm} =$ atmospheric pressure

$p_{in} =$ initial effective stress

$q =$ deviatoric stress

$R =$ plastic strain rate direction tensor

$R' =$ deviatoric plastic flow direction tensor

$r =$ deviatoric stress ratio tensor

$\tilde{r} =$ projection of r on the yield surface along -n

$\tilde{r}^d =$ projection of r on the dilatancy surface along -n

$r_{in} =$ initial load-reversal tensor

$r^M =$ image deviatoric stress ratio point on the memory locus

$\tilde{r}^M =$ projection of r on the memory surface along -n

$\alpha =$ back-stress ratio tensor

$\alpha^M =$ memory back-stress ratio tensor

$\beta =$ dilatancy memory parameter

$\epsilon =$ strain tensor

$\epsilon^{acc} =$ accumulated total strain

$\epsilon_{vol}^p =$ plastic volumetric strain

$\zeta =$ memory surface shrinkage parameter

$\theta =$ relative Lode angle

$\mu_0 =$ ratcheting parameter

$\upsilon =$ poisson ratio

$\xi =$ CSL shape parameter

$\sigma =$ stress tensor

$\psi =$ state parameter

Contents

Abstract v

Nomenclature vii

1 Introduction 1
- 1.1 Offshore structures foundations . . . 2
- 1.2 Loading on Piles . . . 3
  - 1.2.1 Motivation . . . 3
- 1.3 Research Question . . . 4
- 1.4 Methodology . . . 4

2 Literature 7
- 2.1 Monotonic loading on sand . . . 7
  - 2.1.1 Undrained condition . . . 7
  - 2.1.2 Drained condition . . . 8
- 2.2 Cyclic loading on sand . . . 9
  - 2.2.1 Experimental phenomenon of sand ratcheting behavior . . . 9
  - 2.2.2 SANISAND-MS model . . . 11
- 2.3 Monopile response under lateral/ cyclic loading . . . 14
  - 2.3.1 Non Dimensional factors . . . 14
  - 2.3.2 Accumulated Rotation . . . 16
  - 2.3.3 Similarities between the sand behaviour and pile response while applying cyclic loading . . . 19

3 Performance of SANISAND MS model under monotonic and cyclic loading 21
- 3.0.1 Introduction to SANISAND MS . . . 21
- 3.1 Monotonic loading on sand . . . 25
- 3.2 Cyclic Loading in sand . . . 27
  - 3.2.1 Model parameters Analysis . . . 27
- 3.3 Ratcheting parameters (Strain rate and Stiffness rate) . . . 27
- 3.4 Memory surface Parameters . . . 28
  - 3.4.1 Mau . . . 28
  - 3.4.2 Zeta . . . 29
- 3.5 Other Parameters . . . 32
  - 3.5.1 Void Ratio(e) . . . 32
  - 3.5.2 Deviatoric Stress/ average stress(q_a) . . . 34
  - 3.5.3 Amplitude stress(q1) . . . 36
  - 3.5.4 Confining Pressure (p) . . . 37
  - 3.5.5 Strain Superposition . . . 38
  - 3.5.6 Multi amplitude cyclic loading . . . 39
- 3.6 Summary . . . 43

4 3D FE modelling of monopile subjected to lateral loading 45
- 4.0.1 Introduction . . . 45

4.1 Monotonic loading 46
4.1.1 Simulation Plan 46
4.1.2 Pile Geometry effect 46
4.1.3 Soil response under lateral monotonic load 47
4.2 Cyclic Loading 49
4.2.1 Pile Geometry effect 49
4.2.2 The effect of Memory Surface Parameters 51
4.2.3 Loading Factor 51
4.2.4 Visualisation of Cyclic Loading 53
4.2.5 Ratcheting Rates 54
4.3 Summary 55

5 Conclusions **57**
5.1 Conclusions : 57
5.2 Limitations and Recommendations 58

6 Appendix **59**
6.1 Critical surface 59
6.2 Strain superposition 59

List of Figures

1.1 New installation of wind turbines offshores (GWEC market intelligence, July202) 1
1.2 Various types of foundations for OWT 2
1.3 Loading on offshore wind turbine (OWT)[28] 3

2.1 Soil Response during Undrained triaxial test [21] 7
2.2 Loose and Dense sand drained triaxial response [10] 8
2.3 Stress Controlled Undrained cyclic DSS test [48] 9
2.4 Cyclic implicit loading [46] 9
2.5 Soil response during shearing in drained cyclic[46] 10
2.6 Strain accumulation due to varying Relative Density [46] 10
2.7 Schematic of yield,critical,dilatancy and bounding lines [14] 11
2.8 SANISAND MS[32] 12
2.9 Ratcheting Behaviour of sand [28] 13
2.10 Definition for strain accumulation and secant stiffness ([42]) 13
2.11 High drained cyclic loading [30] 14
2.12 Different Laboratory apparatus 15
2.13 Accumulated Rotations cyclic [28] 16
2.14 M_{max}, M_R, M_{min} influence on ξ_b and ξ_c values [27] 17
2.15 Measured displacement as a function of N, R_d,ξ_b,ξ_c [28] 17
2.16 T_b,T_c values [28] 18
2.17 Rate of Rotation accumulation [28] 18
2.18 Comparison between sand and pile behaviour 19

3.1 SANISAND MS model in normalized π plane [31] 22
3.2 Virgin and non virgin loading a)Memory surface expansion virgin loading [30], b)Dilatancy non virgin loading[30] 24
3.3 During drained monotonic loading a) strain b) Volumetric Strain obtained keeping e=0.69 constant and compared with Drained monotonic triaxial tests results by Wichtman(2005) [46] 25
3.4 During drained monotonic loading a) strain b) Volumetric Strain obtained keeping p=200kPa constant and compared with Drained monotonic triaxial tests results by Wichtman(2005) [46] 25
3.5 DSS monotonic loading: a)Shear stress- Shear strain with constant void ratio (e=0.6) b)Shear stress- Shear strain with constant p=100kPa 26
3.6 Results obtained in terms of stress-strain relationships during cyclic loading for varying memory surface parameter a) $\mu = 50$, b)$\mu = 250$ 28
3.7 Results obtained in terms of stress-strain relationships during cyclic loading for varying memory surface parameter $\mu = 500$ 28
3.8 a)Secant Stiffness,b)Accumulated Strain calculated from the cyclic drained loading on sands for 1000 cycles 29
3.9 Stiffness rate and strain rate calculated for memory surface parameters a)(Mau), b) (zeta) 29

3.10 Result obtained during drained DSS a) Shear strains Mau, b) Accumulated strains Mau . . . 30
3.11 Results for varying zeta values in term of stress-strain relationship . . . 30
3.12 Results for varying zeta values in term of stress-strain relationship . . . 30
3.13 Results for varying zeta values in term of a)Secant Stiffness,b)Accumulated Strain 31
3.14 Results for varying zeta values in term of a)Stress strains,b)Accumulated Strain from drained DSS . . . 31
3.15 Results for varying void ratio in term of stress-strain graph for a)e=0.6, b)e=0.7 32
3.16 Results for varying void ratio in term of stress-strain graph for e=0.8 . . . 32
3.17 Results for varying void ratio in term of a)Secant Stiffness,b)Accumulated Strain for 1000 loading cycles . . . 33
3.18 Ratcheting rate for varying Void ratio . . . 33
3.19 Definition of deviatoric stress (qd) and amplitude stress (q1) . . . 34
3.20 Results for varying deviatoric stress in term of stress-strain graph a)qd=30kPa, b)qd=60kPa, c)qd=90kPa . . . 34
3.21 Results for varying deviatoric stress in term of a)Secant Stiffness,b)Accumulated Strain . . . 35
3.22 Results for varying deviatoric stress in term of Ratcheting rate . . . 35
3.23 Results for varying amplitude stress in term of stress- strain graph a)q1=30kPa, b) q1=45kPa . . . 36
3.24 Results for varying amplitude stress in term of stress- strain graph q1=60kPa . 36
3.25 Results for varying amplitude stress in term of a)Accumulated Strain,b)Secant Stiffness . . . 37
3.26 Results for varying amplitude stress in term of Ratcheting rate . . . 37
3.27 Stress- strain graph for varying confining pressures a) p=100kPa, b)p=200kPa 38
3.28 Stress- strain graph for varying confining pressures p=400kPa . . . 38
3.29 Results for varying confining pressures a)Accumulated Strain, b)Secant Stiffness 39
3.30 Results for varying confining pressures as Ratcheting rate . . . 39
3.31 Method used for predicting pile permanent displacement for mixed loading . . 39
3.32 Accumulated strains predicted using Strain superposition for a) Deviatoric stress, b) amplitude stress and compared with actual mixed loads strains . . . 40
3.33 Results for multiple cyclic loading with varying deviatoric stress a)Secant stiffness, b)Accumulated strain . . . 40
3.34 Results for mixed loading with varying deviatoric stress as Stress-Strain relationship . . . 41
3.35 Results for mixed loading with varying deviatoric stress as Stress-Strain relationship . . . 41
3.36 Results for mixed loading with varying amplitude stress as a) Secant stiffness, b) Accumulated strain . . . 41
3.37 Results for mixed loading with varying amplitude stress as Stress-Strain relationship . . . 42
3.38 Results for mixed loading with varying amplitude stress as Stress-Strain relationship (q1=45,30,60kPa) . . . 42

4.1 FE model domain with pile soil discretization . . . 46
4.2 Pile rotation obtained during lateral monotonic loading on FE model for different pile geometries a)pile thickness, b) diameter . . . 47
4.3 Pile rotation obtained during lateral monotonic loading on FE model for different pile geometries a) Pile length, b)load eccentricity . . . 47

4.4 Pile rotation calculated using FEM for different pile geometries while normalizing moment and rotations through Leblanc Normalized formulation 48
4.5 Pile rotation calculated using FEM for different pile geometries while normalizing moment and rotation Achmus formulation 48
4.6 Change in relative density of sand during lateral monotonic loading applied in FEM 49
4.7 Visualization of tilting occurring in pile during lateral monotonic loading applied in FEM 49
4.8 Ratcheting response (Rotation) calculated for different pile geometries (a) Diameter, (b) Length during lateral cyclic loading 50
4.9 Ratcheting response (rotation) calculated for different pile geometries (Load eccentricity) during lateral cyclic loading 50
4.10 Ratcheting response of model under drained cyclic loading while varying Memory surface parameters a) (μ), b)(ξ) 51
4.11 Ratcheting response of model under drained cyclic loading while varying (Cyclic Loading factor) 52
4.12 Cyclic dimensionless function 52
4.13 Distribution of sand relative density after 100 loading cycles for case 1 in table 4.3 53
4.14 Magnitude of strains developed after 100 loading cycles for case 1 in table 4.3 . 53
4.15 Ratcheting Rate against pile geometry a) Diameter, b) Length 54
4.16 Ratcheting Rate against pile geometry Load eccentricity 54
4.17 Ratcheting rate against (Memory surface parameters) a) (μ), b) (ξ) 55

List of Tables

3.1 Parameter studies of memory related parameters (mau, zeta) and other parameters (e, q1, qd, p) 27
3.2 Numerical study program for Multiple cyclic loading 40

4.1 Numerical simulation program to study of effect of pile geometry during Monotonic Loading 46
4.2 Numerical simulation programme to study effects of varying pile geometries and memory surface parameters while Cyclic Loading 50
4.3 Numerical simulation program for varying pile geometries and memory surface parameters corresponding to Tb-Tc values 51

1

Introduction

Depletion of natural resources and the production of fluorinated gasses into the environment are the major factors behind global warming. Global warming is the phenomenon that persists in the alteration of temperature and typical weather patterns in a place. This leads to the melting of the glaciers and an increase in the water level in the oceans. To dwindle the process, researchers had been looking into an alternative source of energy progressively. The world is moving towards renewable energy alternatives for a greener and sustainable future, where offshore and onshore wind farms come into the picture. The first wind turbine used for the production of electricity was built in Scotland in July 1887 by Prof James Blyth of Anderson's College, Glasgow (the precursor of Strathclyde University) [41]. Wind energy results in lower air pollution and carbon dioxide emission. An individual wind turbine has a relatively small physical footprint. It is cost-effective, and the lowest-priced energy source available. Onshore wind turbines can be built on the preexisting farms and ranches as the land occupation is a fraction and the farm owners get rent payments from the owners.

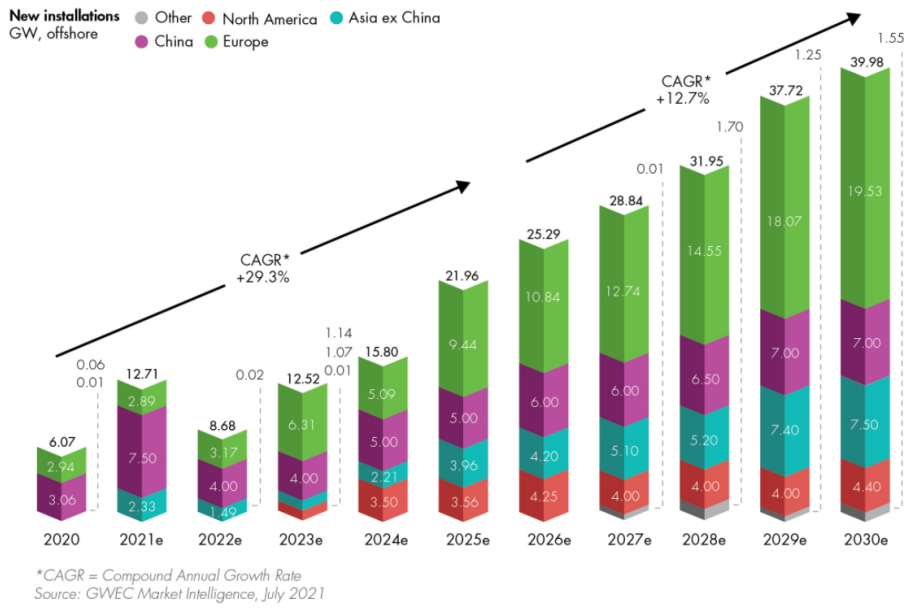

Figure 1.1: New installation of wind turbines offshores (GWEC market intelligence, July202)

Figure 1.1 illustrates the future prediction of the installation of wind turbines globally by 2030. The forecast advertises that 235 GW of new offshore wind capacity will be installed over the next decade. That capacity will be seven times bigger than the current market size and is a 15 percent increase on the previous years forecasts. Europe is currently leading the charts in offshore wind energy (by 84 percent of global installations), having achieved technical and commercial maturity, including the first floating wind farm to generate electricity and together with an emerging zero-subsidy culture. The Chinese wind industry has been developing since 2005, and with well-established rules, the use of a one-stop-shop system in the licensing process, and the establishment of higher feed-in tariffs (FITs), can boost the Chinese offshore wind industry further. The possible role of the USA in the offshore wind industry in the future does not look promising. A more streamlined licensing process, together with a long-term vision enshrined within stable economic incentives, could help to lift the offshore wind industry in the USA [15].

Growth of the offshore wind turbines directs towards the advancement for supporting the turbines under deep waters, increasing the blade size and overall geometry of turbines. Since these are offshore, the factors that can not be neglected are long lengths, foundations supporting structures and effect of varying wave amplitude.Foundation of OWT plays a vital role, since a quarter of the budget is spend here. Advanced Models are able to replicate the soil-structure interaction with different loading scenarios, making it more efficient, reliable and make adjustments according to requirements in designing.

1.1. Offshore structures foundations

Offshore structures overlooks various problems like unusual soil conditions, applied loads, expensive site investigations, harsh environment loads (winds,waves,ice) etc. And its foundations can be either floating or immersed inside soil depending upon the sea depth and distance from the sea shore.

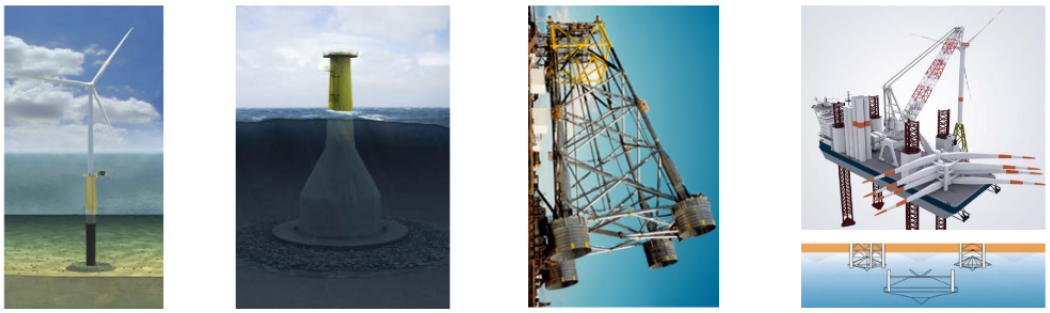

Figure 1.2: Various types of foundations for OWT

The most common types of foundations are piles, gravity foundations, suction caissons, and spud cans 1.2. For shallower depths mostly 40m monopiles and gravity foundations are used for supporting OWT. But for deep greater than 50m, suction caisson and spud can type of foundation are attached to OWT. Monopiles in comparison to other OWT foundations have less complicated designs, easy to transport and install. The anticipated lifetime of a monopile is 20 -25 years with various loading cycles. Monopiles are the most common OWT foundations installed in the north sea.

1.2. Loading on Piles

Monopiles are stiff piles with large diameters and can be driven in the sea bed up to 20-30m. The cost-effectiveness of the pile depends on the site conditions. Designing a monopile is a tricky task in terms of magnitude and characteristic loading. An OWT is subjected to strong cyclic loading not only during extreme conditions but also during normal conditions. This action can cause rotation in the tower of the turbine declining its ultimate strength and in the long term affecting the other parts (blades, machine components) of the wind turbines. Hence, it becomes essential to look into the effects of cyclic loading. Figure 1.3 illustrates the proportions of the OWT with a monopile foundation. H represents lateral loads, L shows the length of the pile, and e, tower length above the pile head.

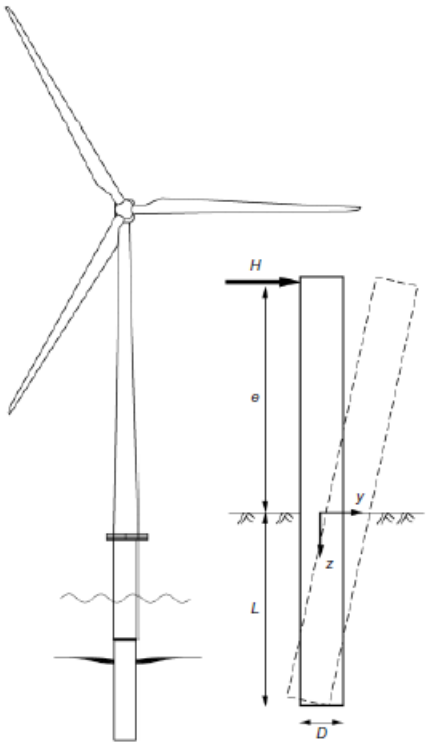

Figure 1.3: Loading on offshore wind turbine (OWT)[28]

1.2.1. Motivation

Offshore wind turbine are subjected to different loading condition through out their life time that comes from natural winds, currents, self weight and earthquakes. Installation and operations also cause loads and moments impose cyclic loading on the piles. Repetitive lateral loading causes tilting (Rotation) from the initial vertical alignment and stiffening of the sand around the foundation. Offshore structure are designed for soft stiff structure with 1P and 3P (.3-1 Hz) frequency of rotor rotation and blade. To limit the rotation, foundations are restricted to rotate only 0.5 degrees. This helps the manufactures of the monopile to design the foundation according to the tolerance limit.

A safe design of Offshore wind turbine can be achieved by taking into account the cyclic loads on monopile performance. With the empirical data and standards provided by oil and gas industry, monopile can be designed. The ultimate loading condition needs to be taken account for designing a pile ([43]). The design of monopiles based on necessary data (i.e. the least amount of data), namely site characteristics (wind speed at reference height, wind turbulence

intensity, water depth, wave height and wave period), turbine characteristics (rated power, rated wind speed, rotor diameter, cut-in and cut-out speed, mass of the rotor-nacelle-assembly) and ground profile (soil stiffness variation with depth and soil stiffness at one diameter depth) ([5]). Another design method to introduce an approximate approach for determining the soil stiffness of sand regarding large-diameter monopiles by modifying the initial stiffness of the API, DNV p-y formulation. This modification introduces both a stress level and a strain level correction derived on basis of sound theoretical considerations without introducing new empirical parameters([22]).

The purpose of this report is to correlate the responses between cyclic sand behaviour and long term monopiles responses (accumulated tilt) under cyclic lateral loading through 3D Finite element Modeling using Opensees platform. The SANISAND-MS model proposed by Liu (2019) [30] is used to simulate the high cyclic sand behaviour and is employed to study the ratcheting behaviour of sand by varying memory surface parameters. Then, the effect of pile geometry on the monopile response was investigated by changing the pile diameter, thickness, length, and load eccentricity. At last, these two groups of elements (sand property and pile geometry) will be further analyzed and discussed about their influence on empirical equations for predicting pile accumulation geometry.

1.3. Research Question

From the past research on the lateral response of the monopile, laboratory/ field experiments were widely conducted, but they are quite expensive and do not consider different sand properties and also limited to varying pile geometries. Therefore, conducting numerical modelling is a suitable way to extend the research work. Hence, these are several opening questions which deserves and are possible to investigate in this thesis work:

1. What changes can be recognized in terms of sand ratcheting behavior based on the SANISAND-MS model through altering memory surface parameters ?
2. What is the response of the monopile under cyclic lateral loading when changes in memory surface parameters are executed?
3. What can be illustrated from varying monopile geometry under monotonic and cyclic loading regarding ratcheting behavior?
4. How do the memory surface parameters and the pile geometry influence the empirical equation for predicting the accumulated rotation of monopile?

.

1.4. Methodology

The main objective of this thesis is to study the effects of lateral cyclic loading on offshore monopiles in sand. And in order do so firstly literature study had been conducted in second chapter. Literature study provides us with the overview of the essential questions that are needed to be understood for this thesis starting with the responses of sand under cyclic loading and better grasp about the ratcheting behavior. Next part of this section talks about the constitutive model SANISAND-MS and its basic principles that helps in replicating the ratcheting behavior in sand. And finishes with effects of cyclic loading on monopiles in terms of pile rotations.

In third chapter, a fairly new constitutive model SANISAND-MS has been explored for computing ratcheting behavior in drained sand conditions. Initially the model has been calibrated

against experimental results. Then ratcheting behaviour is studied for changes in memory surface parameter broadly. Later the model has been calibrated to study effects of confining stress, void ratio, amplitude stress and deviatoric stress. And at last study of accumulated strain under multiple load parcels and its validate the suitability of miners rule based empirical method has been done for 1000 loading cycles.

For fourth chapter, a simulation software OPENSEES had been adopted for numerical modeling. The finite element model helps in recreating soil-monopile domain. Previously discussed constitutive model SANISAND-MS was also introduced in this FEM to investigate the ratcheting effects through accumulated rotations/ tilt. Initially model was computed to look into the effects of memory surface parameters. The next step was to investigate ratcheting response with the influence of pile geometries. And at last the model was used to analyse the empirical equations proposed for predicting the long term monopile during lateral loading for varying pile geometries and memory surface parameters.

In last chapter, conclusions are made according to the research questions discussed previously with the limitations and future scope.

2

Literature

This chapter acknowledges the literature and the background knowledge required to understand the thesis. It includes the work and research done previously on the loading sand and monopiles. Firstly, both drained and undrained behaviour of sand will discussed under monotonic and cyclic loading.

2.1. Monotonic loading on sand

Responses of sand in dense and loose conditions varies and for monotonic loading and the most convenient way is to do a triaxial test. Triaxial test is fast and convenient to find out the strength of the soil sample.

2.1.1. Undrained condition

Figure 2.1, illustrates results of the undrained triaxial test in which water content is not allowed to leave sand sample while shearing [21]. This test consist of two phases: First phase is consolidation phase in which isotropic stress is applied while leaving the sample in drained condition and later, shearing the sand sample under undrained conditions.

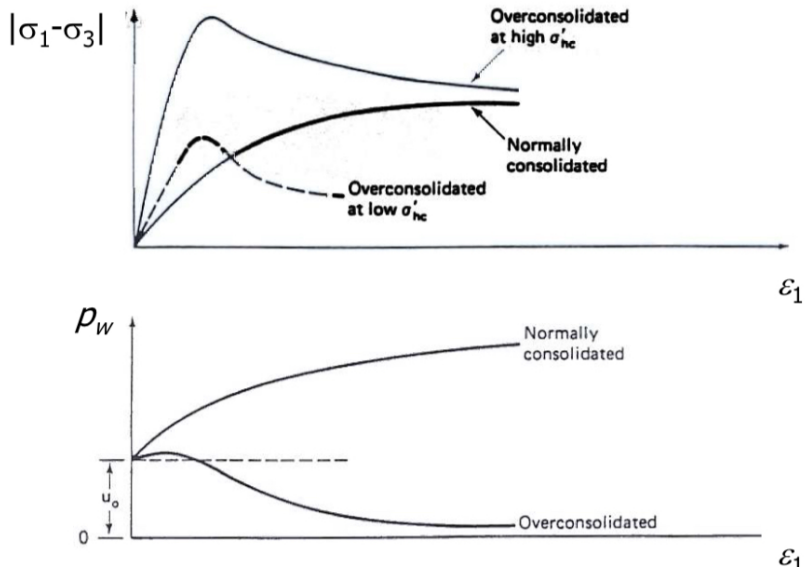

Figure 2.1: Soil Response during Undrained triaxial test [21]

Applying deviatoric stress in dense sand firstly hardening, and later softening of sand can be observed until critical state is reached. For loose sand samples, compressive behaviour of sand is noted. While shearing, pore water pressure is measured in the sample [19]. In normally consolidated sand, positive pore pressure are generated which leads to decrease in the strength and later to the failure. For over consolidated or dense sands, negative pore pressure is generated leading to increase in strength of soil while applying deviatoric stress.

2.1.2. Drained condition

During draining condition, water is allowed to drain in both consolidation and shearing stages. Figure 2.2 illustrates that peak strength is achieved keeping the cell pressure low under dense sand or over consolidated clay. And for the loose sand or normally consolidated clay do not tend to show any peak strength while applying [10]. Since water in between the soil is drained out, volume change is observed in the sample. Loose sands tend to show compression behaviour under drained triaxial loading whereas dense sand firstly compress and then starts to dilate up to no further volumetric change condition.

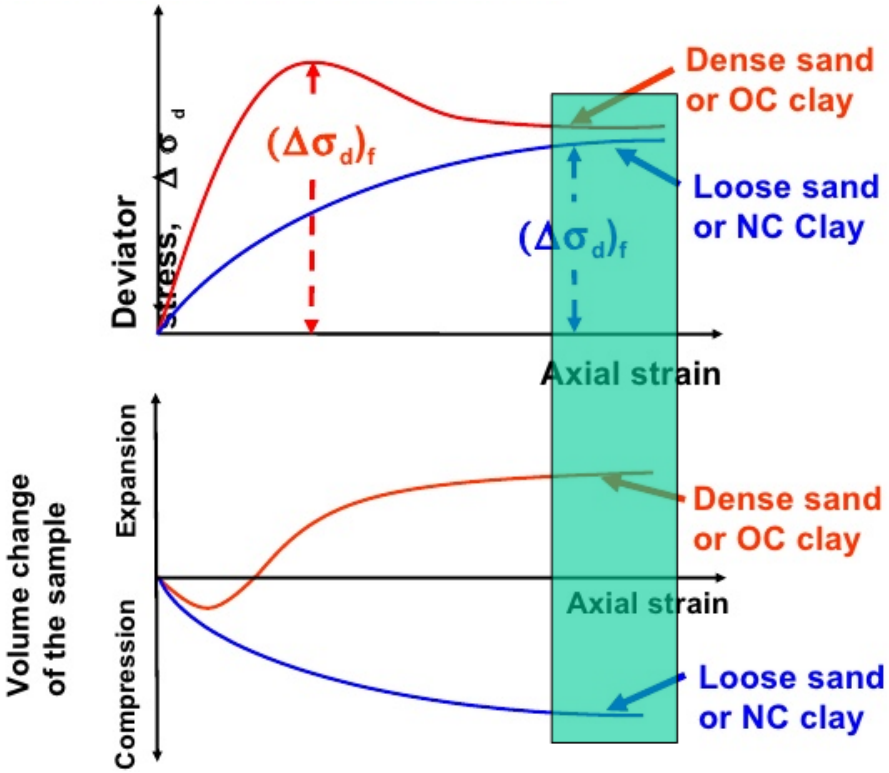

Figure 2.2: Loose and Dense sand drained triaxial response [10]

2.2. Cyclic loading on sand

Offshore wind, currents, earthquakes can cause the cyclic loading. It can lead to generation of pore pressures in soil, accumulation of the strains, damping, energy dissipation and formation of hysteresis. This can further cause reduction in soil stiffness, strength and eventually liquefaction [47] . With the increase in the amplitude of loading, higher will be the damping ratio.

2.2.1. Experimental phenomenon of sand ratcheting behavior

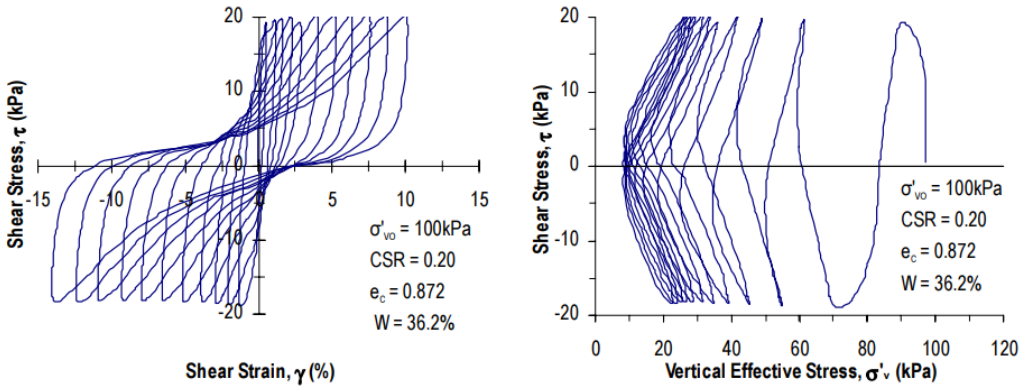

Figure 2.3: Stress Controlled Undrained cyclic DSS test [48]

Figure 2.3 is a stress controlled Undrained cyclic DSS test [48]. The left graph shows hysteresis cycle with generation of more and more irreversible shear strains when shear stress is applied. The right graph illustrates that with the increase in number of cycles, the vertical effective stresses keeps on decreasing due to generation of pore pressure and after the n number of cycles, sample losses its complete strength and it starts to liquify.

Drained cyclic loading are replicated on the basis of critical state theory. Finite element calculations are done to understand the sand response. High-cycle accumulation (HCA) model is proposed to duplicate the behavior. Drained cyclic loading is divided into two types: implicit and explicit.

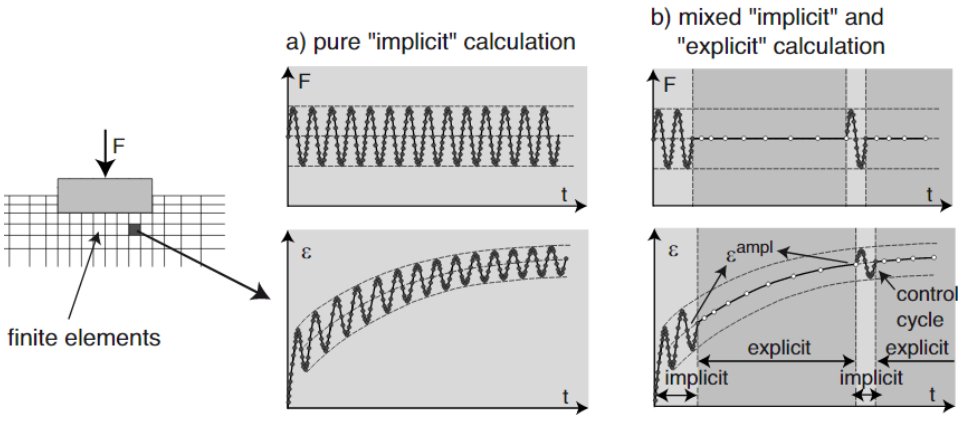

Figure 2.4: Cyclic implicit loading [46]

During implicit cyclic loading, the number of cycles are less than 50 and with increase in the cycles the residual strain increases whereas strain accumulation rate decreases ([46]. For

Explicit cyclic loading, the number of cycles are greater than 50 and a strategy where initial cycles are implicit and later are explicit is used. Most implicit constitutive models predict an almost linear increase of residual strain with increasing number of cycles ($\epsilon_{acc} - N$), which is contrasted by drained cyclic tests which usually show decreasing strain accumulation rates with increasing number of cycles ($\epsilon_{acc} - lnN$). Density, grain size distribution, average stress, amplitude loading, and preloading cyclic history are the important parameters that determines stiffness and strain rate accumulation in sand.

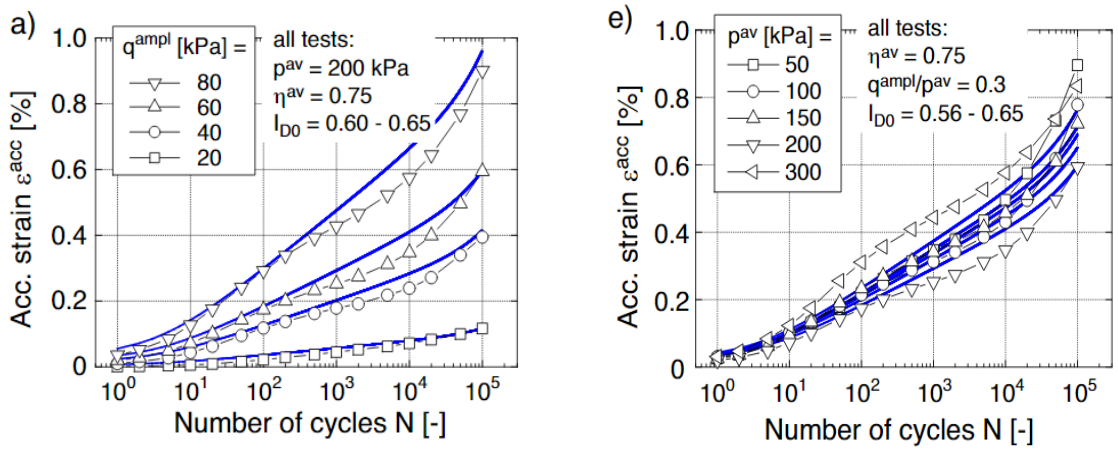

(a) Strain accumulation due to varying amplitude stresses (b) Strain accumulation due to varying cyclic stress history

Figure 2.5: Soil response during shearing in drained cyclic[46]

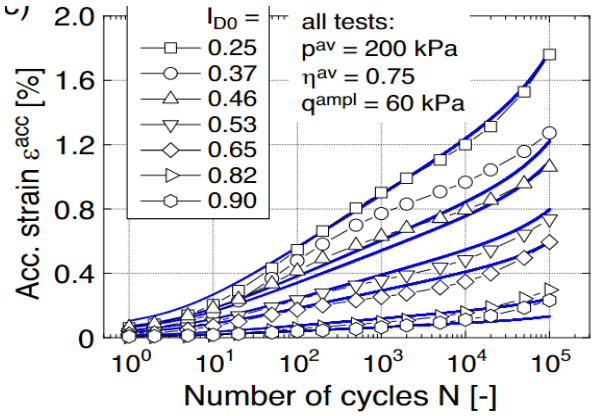

Figure 2.6: Strain accumulation due to varying Relative Density [46]

Critical state

The concept of state relates to the density of material in relation to the critical density (critical state). Critical state is the situation where no further change in volume is observed in material on shearing. It is not the state of failure. Introduced in 1985, it is denoted by ψ [8] where e is void ratio and e_c is critical void ratio 2.1.

$$\psi = e - e_c \tag{2.1}$$

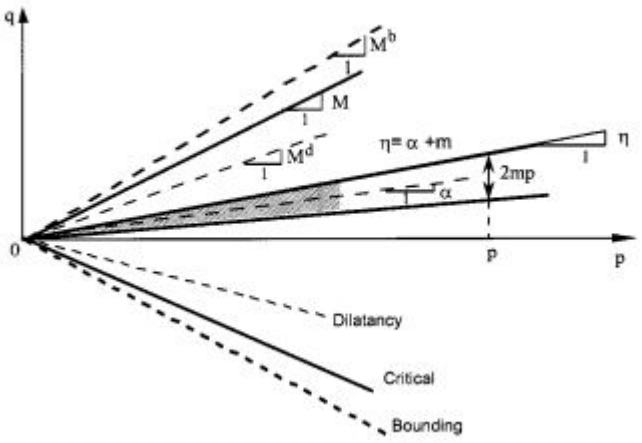

Figure 2.7: Schematic of yield,critical,dilatancy and bounding lines [14]

Sand, in particular reach that state where they neither compact nor dilate on shearing. At critical state ($e = e_c$) $\psi = 0$, loose sand $\psi < 0$, which is the situation below critical state. And for dense sand $\psi > 0$, above the critical state, soil will try to dilate while shearing. Figure 2.7 illustrates the scenario related to the dense sand, because while shearing sand will firstly compact then reaches to bounding surface and the will dilate, later reaches its critical state [14]. For loose sand bounding surface would be below the critical state.

2.2.2. SANISAND-MS model

Constitutive models are created to replicate the results from soils under various types of loading. And they are able to duplicate the outcomes up to certain extent. The history of constitutive modelling of soil goes way back the simplest model of Hooke's law which formulated basic relationship between stress and strain rates. To formulate (elasto)plastic behavior of soil Mohr-Coulomb law originated or Linearly elastic perfectly plastic (LEPP) model. It served as the backbone of most of the models used in the soil mechanics. Disadvantages of the model were that isotropic and homogeneous behavior,no stress dependent stiffness, dilantancy continued forever etc. Drawbacks of the previous models were resolved with new models like Hardening soil model (HS) and Hardening soil (small) model. These models introduced new parameters that resolved the problem of stiff behavior of soil under very small strains, memory of pre-consolidation stress. They were also able to capture hysteresis in cyclic loading (energy dissipation, damping). Nevertheless, they still had some limitations.

To duplicate the nature of the clays and soft soils, Cam clay model was introduced. It follows the critical state theory with state parameter for different soil densitiesψ. Evolution over

original cam clay was modified cam clay model that introduced stress path dependent stiffness along with loading histories into model making it suitable for normally- consolidated clay. After that comes the soft soil creep model, an updated and improved model with time dependent behavior(creep), compression and shear induced creeps.

Since there were models already introduced to replicate the clay and soft soil behaviors initially, later models were created to show sand drained and undrained responses under various loading. UBC sand model was developed University of British Columbia (UBC) in 1998. It can formulate shear hardening like hardening soil model, under cyclic loading can work out accumulation of plastic strains. It can capture cyclic loading and liquefaction upto some extant. PM4Sand model is another sand model developed in 2015 based on bounding surface plasticity[34]. This model is adapted by correlating case histories and experimental data[35],[3]. It captures the effect of fabric densification and improvement over UBCsand model. Inheriting the bounding surface plasticity from PM4Sand, SANISAND MS model was developed.

SANISAND MS model adapts the basic concept of kinematic hardening/ bounding surface elasticity with an extra introduction of the memory surface[12],[38],[37]. The potential benefits of this model is that, it can retain more information about stress history and effect of repeated loading through evolving and contracting memory surface. It is a geometrical illustration of stress history and covers the region of stress state that soil has experienced already. Memory surface is allowed to change its size and position to replicate change in soil fabric under repeated loading. During drained loading, sand tends to show less effect in terms of soil stiffness then under undrained repetitive loading. And to capture stress- strain response of sand while subjected to repeated number of cycles, this model is helpful.

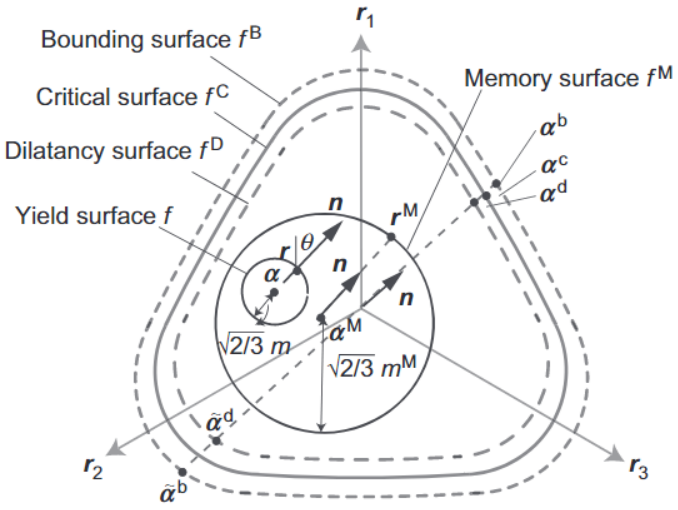

Figure 2.8: SANISAND MS[32]

Memory surface is the circular shape in normalized π plane [6]2.8. There are three rules describing the evolution in the memory surface:

1. Due to experienced plastic strains, memory surface changes in size. More stabilized and stronger soil fabric response can be recognized by the evolution of memory surface with positive plastic volumetric strains corresponding to denser soil state. Where as contraction be associated to negative (dilative) plastic volumetric strains corresponding to loose soil state while shearing. This theory of change in size of memory surface was introduced to formulate soil stiffness increase and decrease during drained and undrained

shearing[38],[18].

2. Yield surface is always enclosed by memory surface[30]. Minimum size of the memory surface can be considered as yield surface.

3. Current stress state surface should always lie with in memory surface.

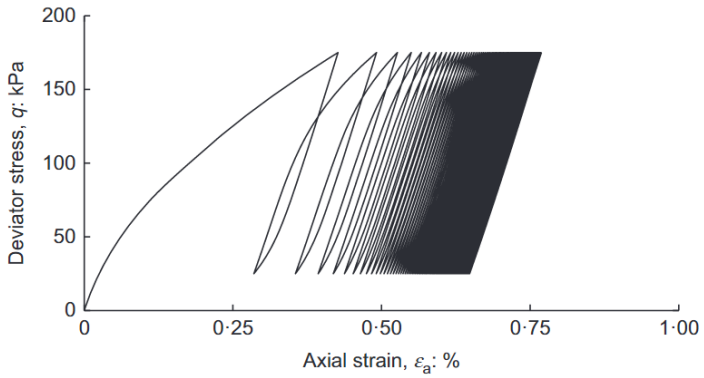

Figure 2.9: Ratcheting Behaviour of sand [28]

Figure 2.9 illustrates ratcheting behaviour of the soil under drained loading using the SANISAND MS([31]). The mechanism of ratcheting occurs during cyclic lateral loading of the pile in sand. After loading the pile to the peak, pile moves back and leaves a small gap open at pile soil interaction. This gap makes the sand grains at the head of pile move downwards along the interface. After reaching the critical depth, the gap is not big enough to move sand further down. As a result sand particles will be pressed into the soil by making advancing movement and moving little by little with every load cycle, resembling ratcheting. Under small loading amplitudes, granular matters reaches to sliding condition and produces irreversible deformation.

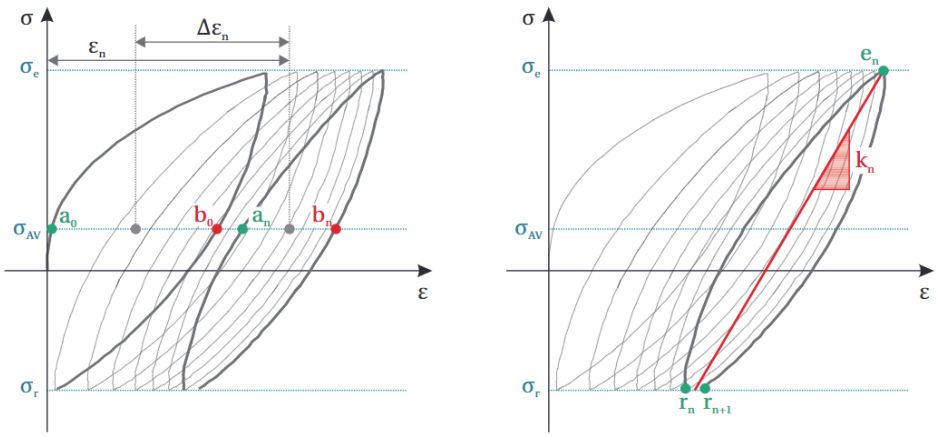

Figure 2.10: Definition for strain accumulation and secant stiffness ([42])

The memory surface is able to captivate the response from ratcheting to shakedown. Ratcheting behaviour is gradual accumulation of the plastic strains under many loading cycles. And strains accumulation ceases after long term cyclic loading. Accumulated permanent strains can be defined equation 2.2 as an average between strains developed in first and last cycle. Secant stiffness can be defined as the slope between the maximum and minimum stress per cycle[26]. Figure 2.10 illustrates the definition of strain accumulation and secant stiffness with number of cycles.

$$\Delta\epsilon_n = 0.5((\epsilon(a_n) + \epsilon(b_n)) - (\epsilon(a_0) + \epsilon(b_0))) \tag{2.2}$$

$$\epsilon_{acc} = \sqrt{2(\epsilon_{xx})^2 + (\epsilon_{zz})^2} \tag{2.3}$$

The gradual sand stiffening with reduced plastic strains can be observed through decreasing area of stressstrain loops. In order to calculate the rate of accumulate strains and secant stiffness, on double logarithmic axes curve fitting tool will be used. Two memory surface parameters introduced in SANISAND MS are μ, ζ.

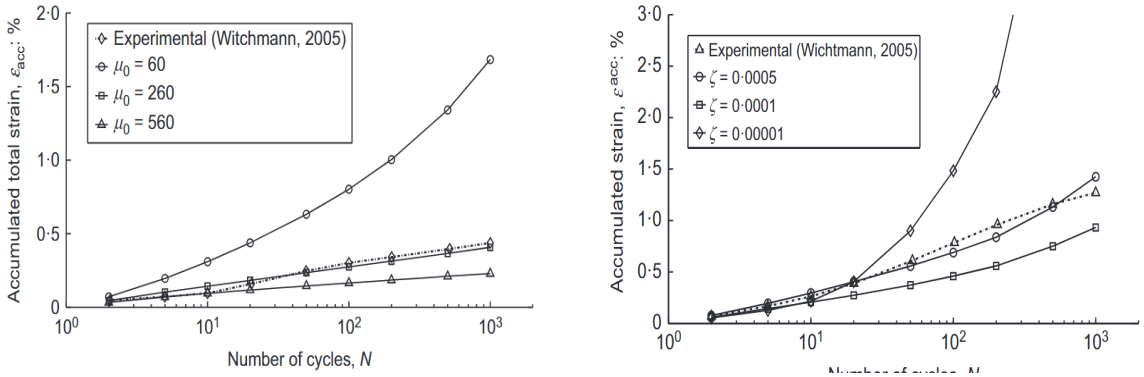

(a) Mu (b) zeta

Figure 2.11: High drained cyclic loading [30]

A comparison has been done in Figure 2.11 regarding the accumulated strains observed by Wichtmann2005 report [46] and SANISAND MS parameters [30]. And it can be observed that both the memory surface parameters are able to replicate strains. μ_0 is the ratcheting coefficient and it can be illustrated that with the increase in the number of cycles, there would be decrease in the strain accumulation rate in soil and as the value of the μ_0 is increasing, the rate of strain accumulation will be decreasing.

2.3. Monopile response under lateral/ cyclic loading

Majority of offshore wind turbines (OWT) in Europe are supported by monopile foundations due to their straightforward design, robust installation and etc [40]. Monopiles are hollow steel structures that might go up to 8 to 10 m of diameter depending on the requirement [36]. Cyclic loading through waves, winds can cause rotation in pile as well as deformation in soils[33]. The lifetime anticipated for the OWT structures is around 20-25 years during which it is faced different types of loading's. The design method opted for the monopiles by DNV (2016) shows uncertainty regarding accounting the effect of cyclic loading on the structure that leads to foundation stiffness with time and prediction of the evolved deformations. And for accurate estimation of fatigue life these estimation are really vital [1], [42],[9],[43]. Discrepancies in the current design approach has lead to many research projects. Various researchers developed different physical apparatus and multi surface plasticity models to explore phenomenological ways to replicate the results of the pile behaviour to the model pile for multiple cyclic loading [1], [7]and also with Empirical formulas based on laboratory work[4],[17],[13], [2].

2.3.1. Non Dimensional factors

To match results of full scale structure with laboratory floor experiments, parameters need to be scaled properly. One of the most common problem recognized here would be loading response

for structures in sand is governed by the frictional behavior due to isotropic stress. And lower isotropic level in laboratory leads to high friction angles[28]. By choosing the appropriate scaling methods such issue can be solved. These scaling laws are addressed uniquely as the dimensionless factors [23].

Moment Loading

$$\tilde{M} = \frac{M}{L^3 D\gamma'} \tag{2.4}$$

Vertical force

$$\tilde{V} = \frac{V}{L^2 D\gamma'} \tag{2.5}$$

Horizontal forces

$$\tilde{H} = \frac{H}{L^2 D\gamma'} \tag{2.6}$$

Rotation (degrees)

$$\tilde{\Theta} = \Theta(\frac{P_a}{L\gamma'})^{0.5} \tag{2.7}$$

Load eccentricity

$$\tilde{e} = \frac{M}{L.H} \tag{2.8}$$

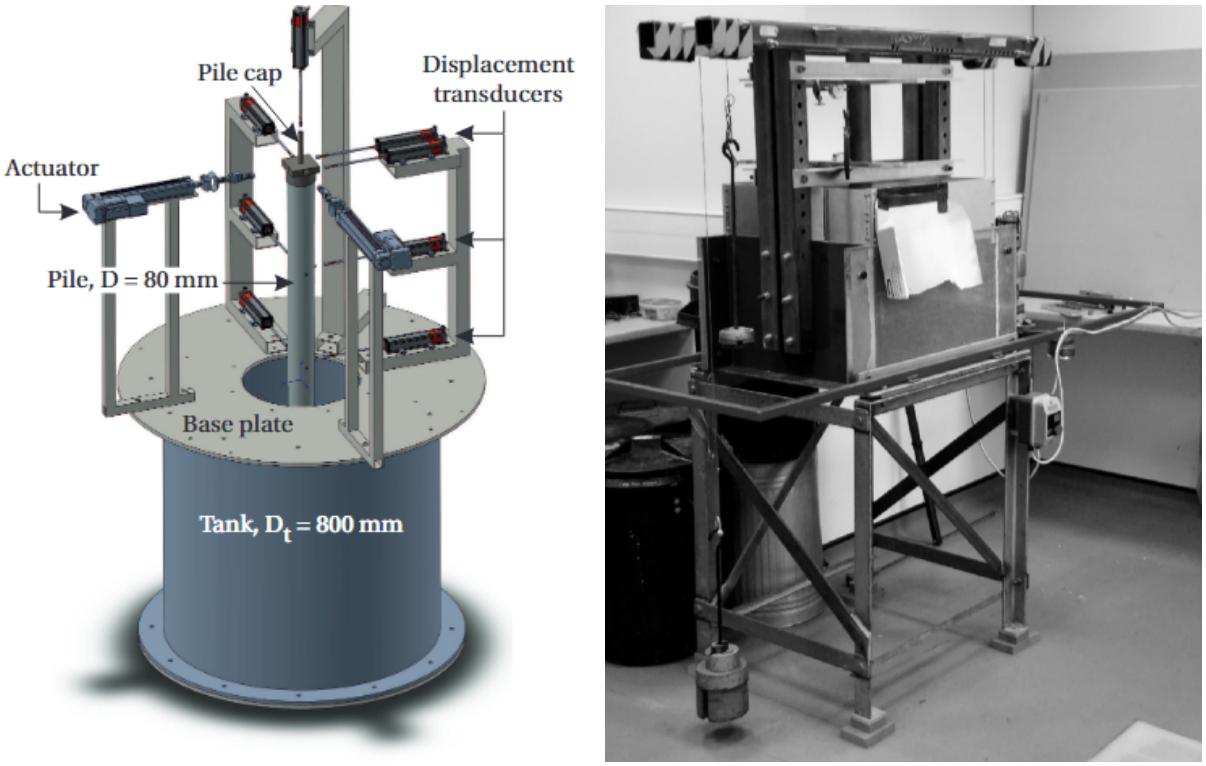

(a) Laboratory apparatus [42]

(b) Fatigue loading rig [28]

Figure 2.12: Different Laboratory apparatus

Scaled models of monopile $1:100$ were set up of various dimensions like rigid hollow pile with smooth outing, length of 320mm, diameter of 80mm and thickness of 5mm [42], stiff

copper monopile scaled upto $1:50$ outer dimensions [28], [1], and 60cm diameter cylindrical steel with depth of 75cm [4]etc to study unidirectional, multi directional and multi-amplitude loading response. High quality measuring device actuators, LVDT are attached to measure pile rotation and displacements. Testing equipment rig are developed as shown in figure 2.12b which consist of a combination of rotating and suspended masses, sand container, motor and steel support structure. This rig is able to produce incremental load, two way loading by adding masses. Figure 2.12a shows another pile arrangement where piles embedded upto certain length by hammering and then 2 electric actuators at fixed eccentricity are used to apply varying lateral loads.

For addressing pile rotation under different loading cycles, two type of sand samples are considered one with loose RD and other dense RD. The results are presented for the 1g laboratory floor model test to evaluate accumulated rotations and stiffness. The equipment used here loaded to series of lateral loads and moments to replicate the loads due to currents, waves and wind peak frequency of offshore waves. The reference magnitudes for ground displacement be 0.1D and for rotation equals to 2 degree. The Loading rig was used first to test the monotonic loading, then in second phase importance of initial curve for cyclic loading, third phase non symmetric continuous cyclic loading and for fourth phase multi amplitude loading.

2.3.2. Accumulated Rotation

Figure 2.13, illustrates $\frac{\Delta\theta(N)}{\theta(s)}$ which is the accumulated rotations while applying moment M (N cycles) [29]. $\Delta\theta(N)$ is difference between the rotation occurred during first and last cycle. And $\theta(s)$ is the maximum strain that occurred during lateral monotonic loading.

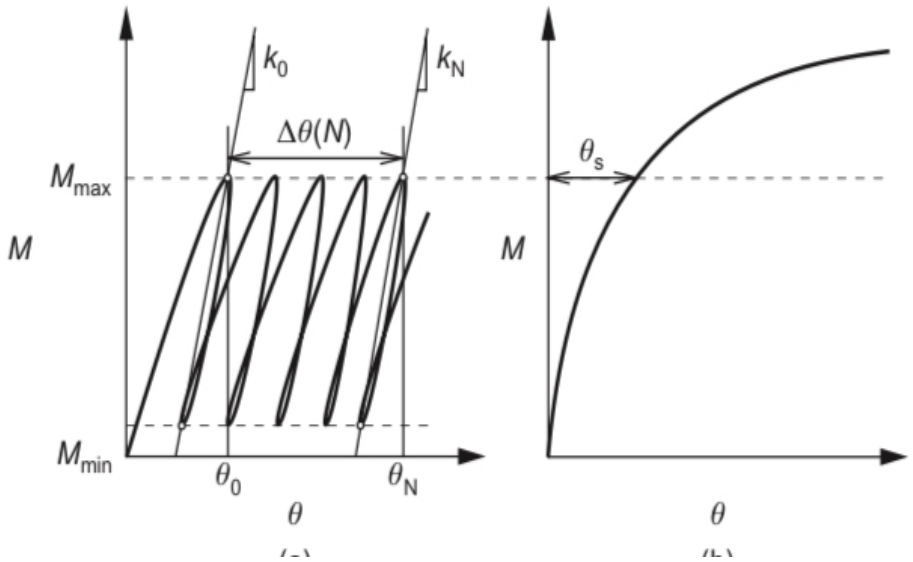

Figure 2.13: Accumulated Rotations cyclic [28]

These cyclic loading tests are characterised by two normalising parameters ξ_b and ξ_c.These independent parameters ξ_b and ξ_c are used to characterise the applied sinusoidal loading where ξ_b represents magnitude of loading and ξ_c represents direction of loading. Figure 2.14 shows that both the factors depends on M_{max}, M_R, M_{min} which is maximum moment, static moment capacity and minimum moment while applying load cycles.

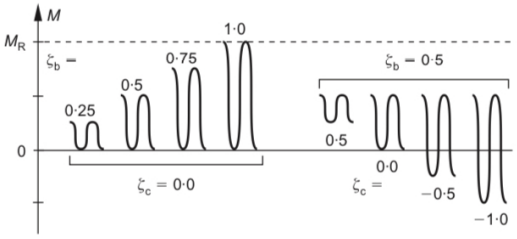

Figure 2.14: M_{max}, M_R, M_{min} influence on ξ_b and ξ_c values [27]

$$\xi_b = \frac{M_{max}}{M_R}, \xi_c = \frac{M_{min}}{M_{max}} \tag{2.9}$$

From the figure 2.15, it can be observed that accumulated rotations seems to be increasing exponentially with the number of cycles and exponential behaviour appears to be working fine for $\xi_c > 0$ in double logarithmic axis. From this observations it was proposed that displacement/ accumulated strains due to cyclic loading can be predicted through equation 2.10.

$$\Delta\theta(N)/\theta_s = T_b(\xi_b, R_d)T_c(\xi_c)N^{\alpha} \tag{2.10}$$

In equation 2.10 T_b,T_c are related directly to dimensionless functions depending on load characteristic and relative density.

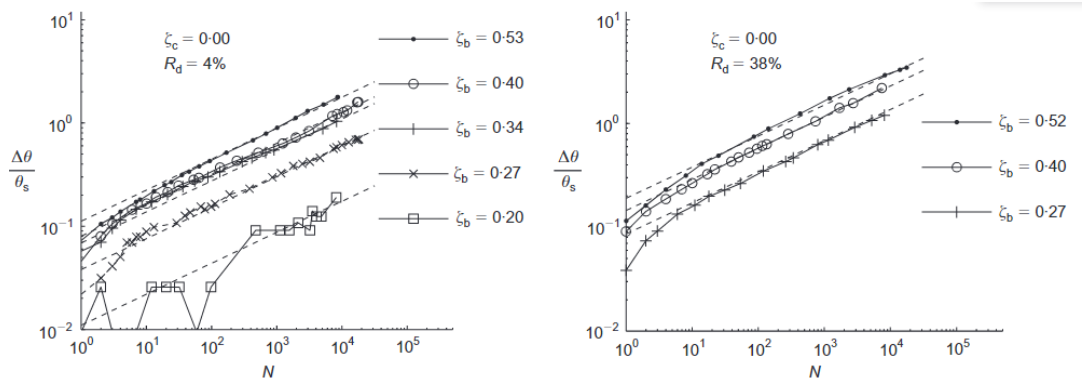

Figure 2.15: Measured displacement as a function of N, R_d, ξ_b, ξ_c [28]

From the figure 2.16 it can be observed that loose sand have low value of t_b as compared to dense sand. Clearly, when ξ_c equals to 1 then t_c will be zero due to static loading no displacements will be accumulated. And during ξ_c equal -1 again t_c will be zero due to equal and opposite forces. α is the ratcheting parameter chosen to show pile response.

Cyclic loading can cause progressive accumulation of the permanent pile rotations and pile head displacement, with additional rotation developed in each cycle reducing as the number of cycle(N) increases [45], [39]. Since permanent rotation are related to relative density and loading stress level, the rate of rotation tends to decrease with increase in cyclic stress loading [28]. From the results of the accumulated rotation with respect to number of cycle, it is possible to calculate the rate of accumulated rotations with the help of power law equation 4.2. The ratio of maximum positive rotation in N cycles with respect to rotation reached in first cycle

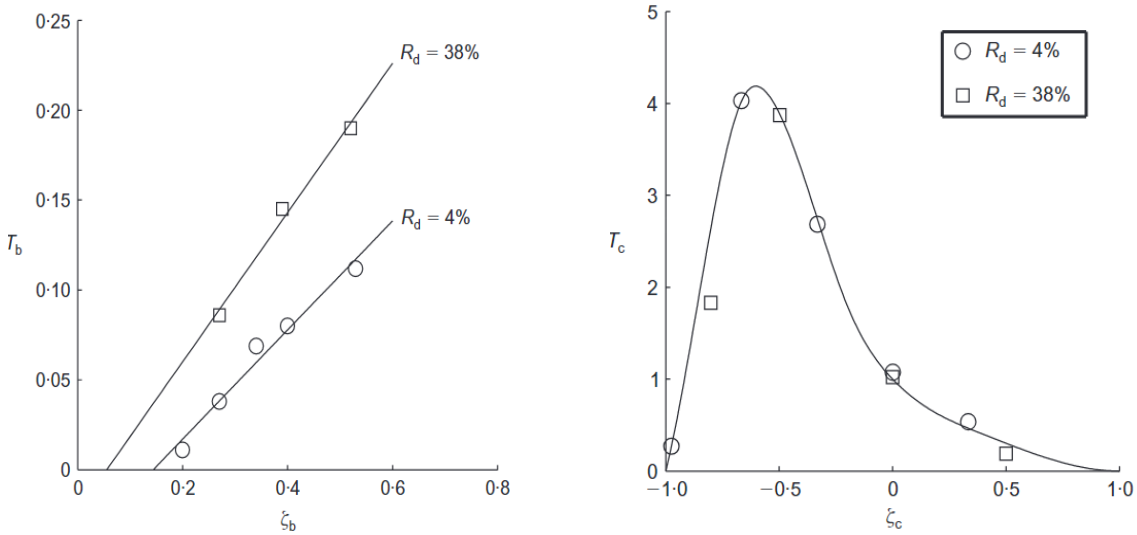

(a) tb-etab (b) tc-etac

Figure 2.16: T_b,T_c values [28]

is power function of N. Here the power coffecient α_r will be determining the rate of rotations with loading 2.17.

$$\theta_N = \theta_1 . N^{\alpha r} \tag{2.11}$$

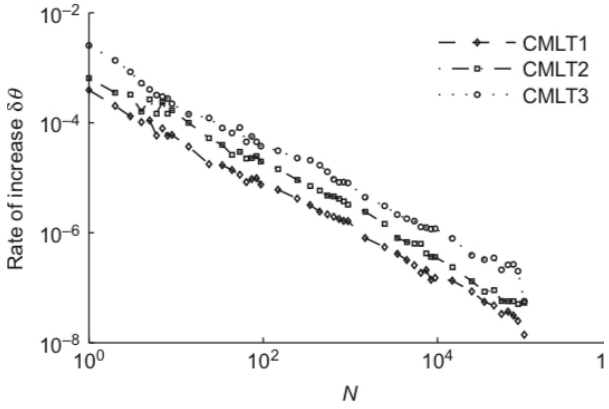

Figure 2.17: Rate of Rotation accumulation [28]

2.3.3. Similarities between the sand behaviour and pile response while applying cyclic loading

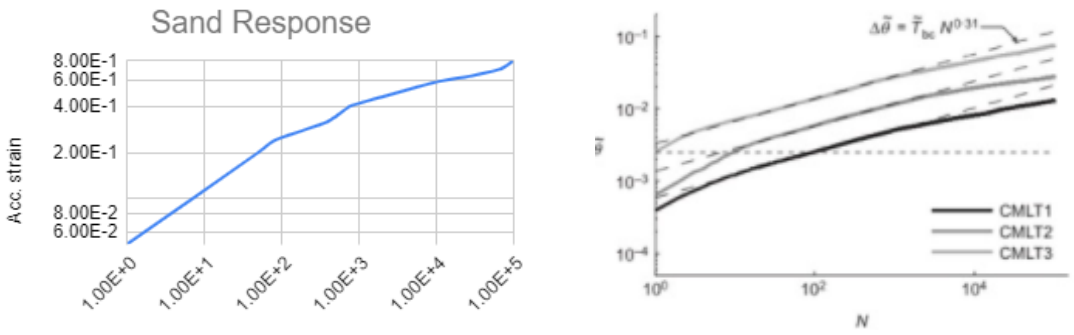

(a) Sand response

(b) Rotation in pile

Figure 2.18: Comparison between sand and pile behaviour

The left figure 2.18 formed between the strain level developed in the sand while loading through N number of cycles shows that the curve is quite linear with the increase in the number of cycles. A similar kind of behavior can be seen in the figure to the right which is the pile response during loading. Instead of strain, rotation is accumulated in the piles which increases with loading cycles. Both the figures shows that the accumulation of strains and rotations decreases with the increase in loading cycles. Hence similar response is followed by the sand and pile while applying cyclic lateral loading.

3

Performance of SANISAND MS model under monotonic and cyclic loading

In geotechnics, methods that are passed on to analyze the monopile responses are field tests, lab tests, physical modeling, and numerical modeling. Field testing requires machinery as well as manpower to collect the data and comprehend the soil condition. Although this method provides the most accurate information, nonetheless it is expensive and time-consuming. A scaled-down method of lab testing is also effective and efficient but collecting the sample of soil and maintaining its integrity is hard. This method can also not comprehend the complete picture of the sub-surface beneath. In the past few years, physical modeling has also become quite a popular option for researchers. It is a competent process of scaling down the prototype to a certain factor and modeling its scaled version with the same properties. But, scaling down is restricted to a certain level like soil grain size seems impossible. It is a comparatively new method with high costing centrifuge equipment, scaling laws, and a lack of research. This has given rise to explore constitutive models for better understanding.

3.0.1. Introduction to SANISAND MS

The SANISAND MS model is the advancement over SANISAND model developed on the concept of memory surface. An assumption is made following the parent model SANISAND that plastic strains occur only with the variation in r value. It is defined as stress ratio $r = s/p$. This step has been taken to describe plastic loci and hardening mechanism effectively on the π plane.

Yield Surface:

For soil elasticity, inside the yield locus model is supposed to behave as (hypo) elastic. The Poisson ratio v and pressure dependent shear modulus are constant. A yield locus is open conical at $f = 0$ with small opening associated with expansion of the back stress ratio α and parameter m.

$$\sigma = \mathrm{E}\epsilon \tag{3.1}$$

$$p = \sigma_1 + 2\sigma_3/3, s = \sigma_1 - \sigma 3 \tag{3.2}$$

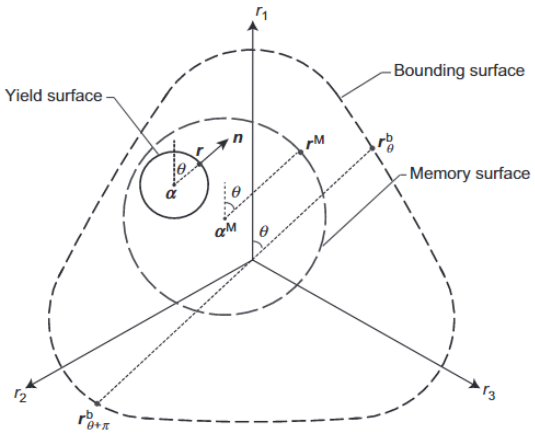

Figure 3.1: SANISAND MS model in normalized π plane [31]

$$f = \sqrt{(s - p\alpha) : (s - p\alpha)} - \sqrt{2/3}mp = 0 \tag{3.3}$$

Plastic strains occurs when r is on yield surface and dr is pointing outwards whereas when r is inside yield surface only elastic strains occurs.

Critical state locus:

To develop the locus, SANISAND MS model uses fundamentals of critical state soil mechanics theory where $M = q_c/p_c$ at critical point and soil deforms on shearing at fixed stresses. Locus of critical state is assumed in multidimensional $e - \sigma$ space and project on e-p plane.

$$e_c = e_0 - \lambda_c(p_c/p_{at})^{\psi} \tag{3.4}$$

State parameter helps the consecutive model to identify sand behaviour at different densities. $\psi = e - e_c$ state parameter can be stated as difference between void ratio and critical state void ratio.

Flow rule:

Flow rule outlines the development in plastic strains and can be classified as deviatoric plastic strains and volumetric plastic strains:

$$d\mathrm{e}^p =< L > \mathrm{R}' \tag{3.5}$$

R' is the tensors deviatoric plastic flow direction where as D tells us about dilatancy coefficient. For the experimental observation, dense soil senses incremental pore pressure with the number of undrained cyclic loading conditions and hence, a dilatancy coefficient D is also introduced in the flow rule. The fabric starts to dilate.

$$de^p_{vol} =< L > D \tag{3.6}$$

Bounding surface:

According to the hardening law, back stress ratio α (axis of the yield locus)is supposed to evolve. The equation 3.7, centre of the yield locus translates in the π plane along $(r_\theta^b - r)$ direction. The magnitude of the back stress ratio is amplified with hardening factor h.

$$d\alpha = \frac{2}{3} < L > h(\mathrm{r}_\theta^b - \mathrm{r}), K_p = \frac{2}{3} ph(\mathrm{r}_\theta^b - \mathrm{r}) : \mathrm{n} \tag{3.7}$$

r_θ^b parameter is used here to navigate the projection of the current stress ratio on the bounding surface. ψ and material constant n^bin the equation 3.8 helps modulating the size of the bounding surface.

$$r_o^b = \sqrt{(2/3)g}(\theta) M exp(-n^b \psi) n \tag{3.8}$$

Memory surface:

Memory surface captures the link between gradual change in fiber and soil stiffness. The influence of fabric effects on soil stiffness in memory surface is represented by μ_0, h is for hardening coefficient (equation3.9). The soil stiffness not only considered to rely on relative distance between current stress stage(r)and its image on bounding surface(r^b) but also in image on memory surface(r^M). The contractive behaviour (Figure 3.2) leads to stiffer soil behaviour and more stable soil fabric configuration hence the memory surface expands. During expansion, virgin loading happens which is the state when yield and memory surface are tangential to each other at current stress point[32].

$$h = \frac{b_0}{(r - r_{in}) : n} \exp \mu_0 (\frac{p}{p_0})^{0.5} (\frac{b^M}{b_{ref}})^2 \tag{3.9}$$

Under non virgin loading, the memory surface act as an additional bounding surface. Soil stiffness increases by b^M in equation 3.9 between yield and memory surface. In contrast, dilative soil behaviour shows fabric damage and soil looses its stiffness. This leads to the shrinkage in memory surface. The process of contraction occur only due to negative volumetric plastic strains production and can be represented through parameter (ζ).

$$D = A_d(r^d - r) : n, A_d = A_0 \exp \beta \frac{< b_d^M >}{b_{ref}} \tag{3.10}$$

Here A_o is 'intrinsic' dilatancy parameter and β is dilatancy memory parameter. When b_d^M>0, soil experienced dilation during previous loading,implying contractive bias and enlarges D due to larger A_d >1. b_d^M<0,soil fabric is biased towards dilation bias implying A_d =1

The State parameter (ψ) concept is adopted to measure distance from critical state conditions. Equation 2.1 states that state parameter is void ratio subtracted by void ratio critical. Value of e_c can be obtained from Equation 3.11 where λ_c,p_a are constants. A wide range of ψ can be obtained with p_c, e_0.

$$e_c = e_0 - \lambda_c (p_c / p_{at})^\psi \tag{3.11}$$

$$M^b = M.exp(-n^b \psi) \tag{3.12}$$

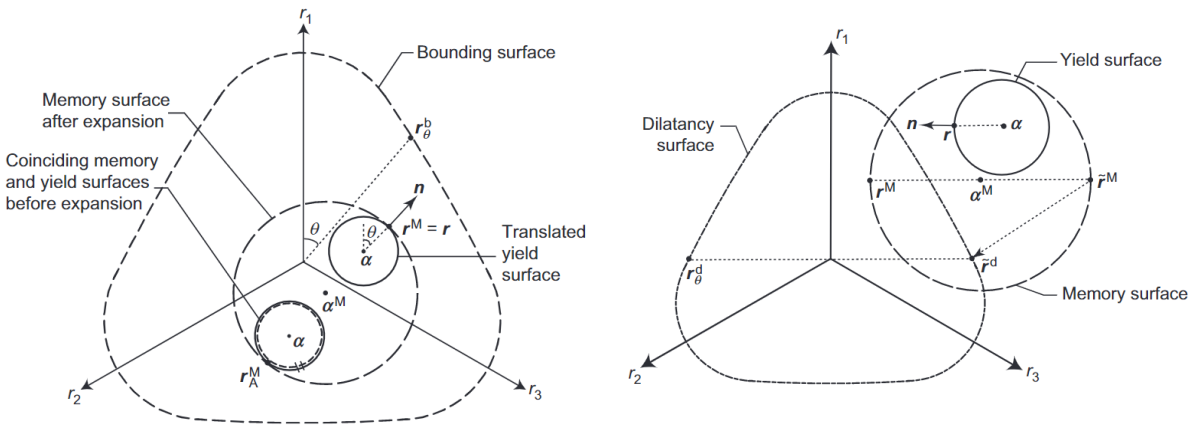

Figure 3.2: Virgin and non virgin loading a)Memory surface expansion virgin loading [30], b)Dilatancy non virgin loading[30]

$$M^d = M.exp(n^d \psi) \tag{3.13}$$

$$r_o^d = \sqrt{(2/3)g}(\theta) M exp(n^d \psi) n \tag{3.14}$$

r_o^d employs in equation 3.14 the projection of dilatancy locus on normalized π plane. $(r_0^d - r)$ imply the distance between memory and dilatancy surface 3.10and can also be written as $\tilde{b}_d^M$

$$dm^M = \sqrt{3/2} d\alpha^M : n - (m^M/\zeta) f_{shr}(-d\epsilon_{vol}^p) \tag{3.15}$$

$$h^M = 0.5[\frac{b_0}{r^m - r_{in} : n} + \sqrt{3/2}(\frac{m^M f_{shr} < -D >}{\zeta(r_0^b - r^M) : n}] \tag{3.16}$$

2.7 shows the Dilatancy, critical and bounding lines between mean pressure and deviatoric stress. If the sand is dense, the ψ would be negative or < 0 and applying that value to Equation 3.12and 3.13 will show $M^d < M < M^b$ and visa versa for loose sand. Equation 3.15 demonstrates the effect of critical state parameter to calculate the plastic volumetric strains. In loose sand, dilative behaviour can not be observed and hence the zeta part of Equation 3.16 will not be activated. This gives the conclusion that zeta parameter works for dense sands.

3.1. Monotonic loading on sand

The calibration of the SANISAND MS model is done for the drained monotonic loading. The parameters opted to do the analysis are void ratio (e=0.69) and confining stress (p=200kPa) by mean of deviatoric stress-axial strain (q_d-ϵ_a) and volumetric strain-axial strain ($\epsilon_{vol} - \epsilon_a$)graphs. The calibration of model parameters is done against the Drained monotonic triaxial tests results by Wichtman(2005) [46].

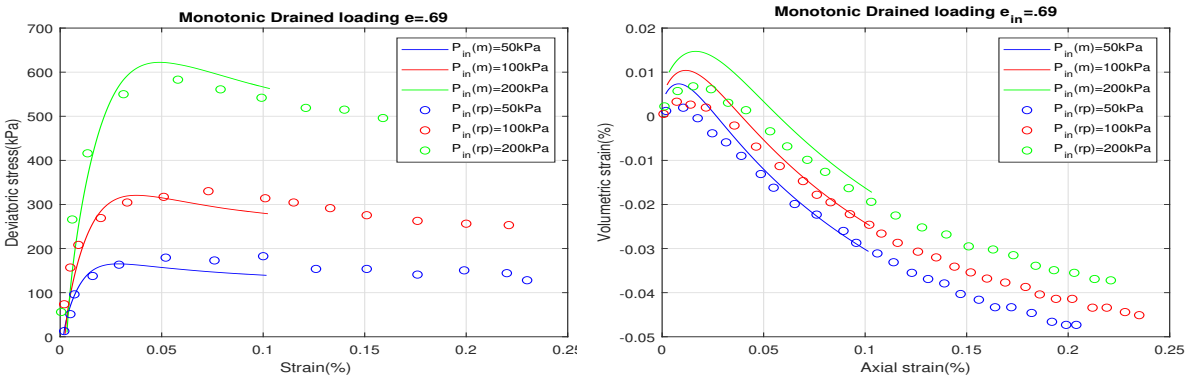

Figure 3.3: During drained monotonic loading a) strain b) Volumetric Strain obtained keeping e=0.69 constant and compared with Drained monotonic triaxial tests results by Wichtman(2005) [46]

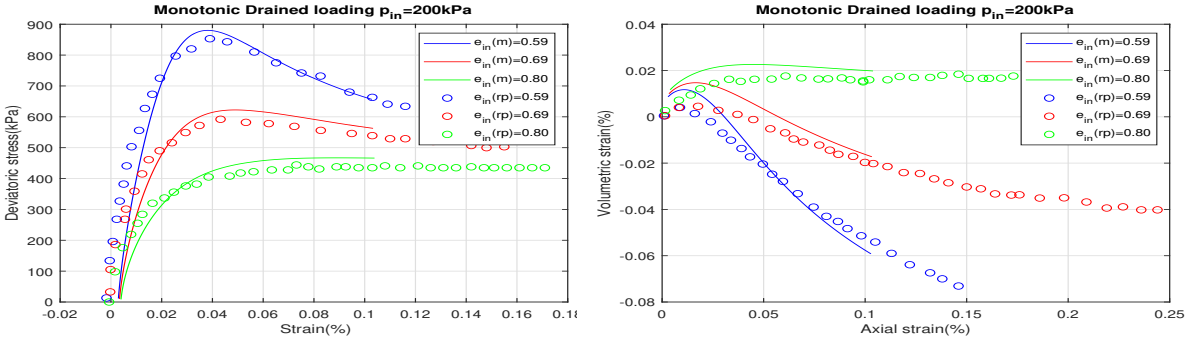

Figure 3.4: During drained monotonic loading a) strain b) Volumetric Strain obtained keeping p=200kPa constant and compared with Drained monotonic triaxial tests results by Wichtman(2005) [46]

The results for monotonic loading are illustrated in 3.3 and 3.4. For the e=0.69, model predicts quite accurately axial strains and volumetric strains for small stress level where as it over estimates strains for higher confining stress. With the increase in the confining stress, peak is more visible for loose sand while shearing. And soil tends to compress while stress is applied. In terms of constant confining stresses, SANISAND-MS model seems to predict the strains and volumetric strains moderately well. Figure 3.4 illustrates that denser the soil, peak is obtained with same confining stress. Hence, from both the graphs3.3 and 3.4 it can be concluded that SANISAND-MS model is able to replicate the drained triaxial behavior.

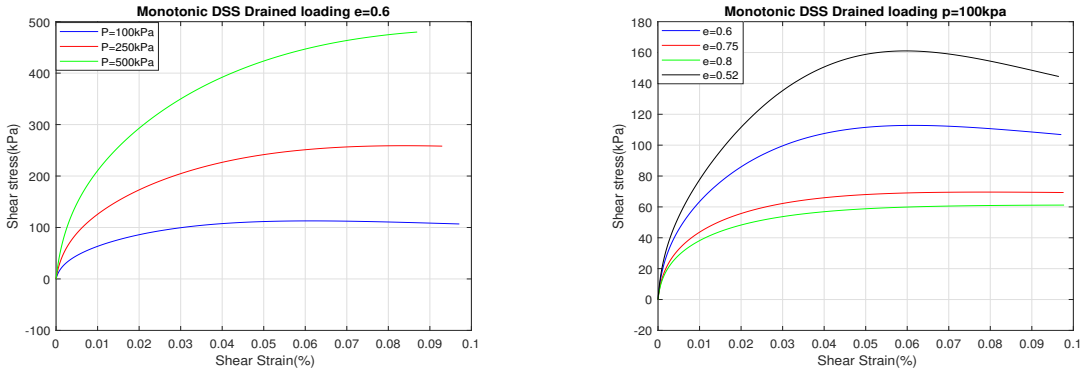

Figure 3.5: DSS monotonic loading: a)Shear stress- Shear strain with constant void ratio (e=0.6) b)Shear stress- Shear strain with constant p=100kPa

Another typically DSS test is employed to replicate the strains developed during shearing soil through SANISAND MS model for loose sand condition under drained monotonic loading. Figure 3.5 illustrates strains evolved during shearing sand.

Here, the model is implemented for varying void ratios and varying confining stresses. Figure 3.5 on left indicates that shear strength is higher for higher vertical stresses. And Figure 3.5 on right, conveys that for loose soil, less will be its shear strength and more easily it will get damaged while shearing.

3.2. Cyclic Loading in sand

3.2.1. Model parameters Analysis

A table 3.1 is used to analyze the working of the SaniSand MS model under Drained Cyclic loading. Various factors that affect the behavior of sand during the computation of the model are Memory surface parameters like Mau(μ), Zeta(ζ), and other parameters like Void Ratio(e), Confining stress(p) and Deviatoric stress (q) regarding ratcheting rate for strain as well as stiffness are studied.

Table 3.1: Parameter studies of memory related parameters (mau, zeta) and other parameters (e, q1, qd, p)

No.	p(kPa)	μ	ζ	e	q_d(kPa)	q_1(kPa)	Ratcheting rate(strain)	Ratcheting rate(stiffness)
1	100	50	0.0001	0.48	120	30	0.6939	4.042
2	100	50	0.0005	0.48	120	30	0.253	3.306
3	100	50	0.001	0.48	120	30	0.4015	3.197
4	100	50	0.0001	0.6	30	30	0.253	3.211
5	100	50	0.001	0.6	30	30	0.253	3.211
6	200	50	0.001	0.6	30	30	0.3052	3.565
7	200	50	0.001	0.7	30	30	0.2427	3.737
8	200	50	0.001	0.8	30	30	0.2536	4.348
9	100	50	0.0001	0.7	30	30	0.2396	3.601
10	100	50	0.0001	0.7	60	30	0.26	3.951
11	100	50	0.0001	0.7	90	30	0.3123	4.463
12	100	50	0.0001	0.7	30	30	0.2396	3.601
13	100	250	0.0001	0.7	30	30	0.1298	1.005
14	100	500	0.0001	0.7	30	30	0.09849	0.6401
15	100	250	0.0001	0.6	30	30	0.1438	0.9108
16	200	250	0.0001	0.6	30	30	0.1785	1.065
17	400	250	0.0001	0.6	30	30	0.2124	1.303
18	200	250	0.001	0.6	30	30	0.1785	1.065
19	200	250	0.001	0.6	30	45	0.1542	1.052
20	200	520	0.001	0.6	30	60	0.1359	1.062

3.3. Ratcheting parameters (Strain rate and Stiffness rate)

Equation 3.17 pictures the strains in sand through out cyclic loading where, ϵ is for strains, A is constant, N is for number of cycles and α depict strain rates. In the similar manner, equation 3.18 portray stiffness in sands during cyclic loading. And in this equation p_1 denote the stiffness rate. To understand strain and stiffness rates briefly 2.10

$$\epsilon = A * N^{\alpha} \tag{3.17}$$

$$k = p_1 ln(N) + p_2 \tag{3.18}$$

With curve fitting tool in MATLAB, values of the ratcheting parameters can be achieved directly.

3.4. Memory surface Parameters

3.4.1. Mau

μ a memory-related parameter, that takes care of the ratcheting response of the soil. It is related to the soil stiffening under drained cyclic conditions and undrained build-up pore pressures.

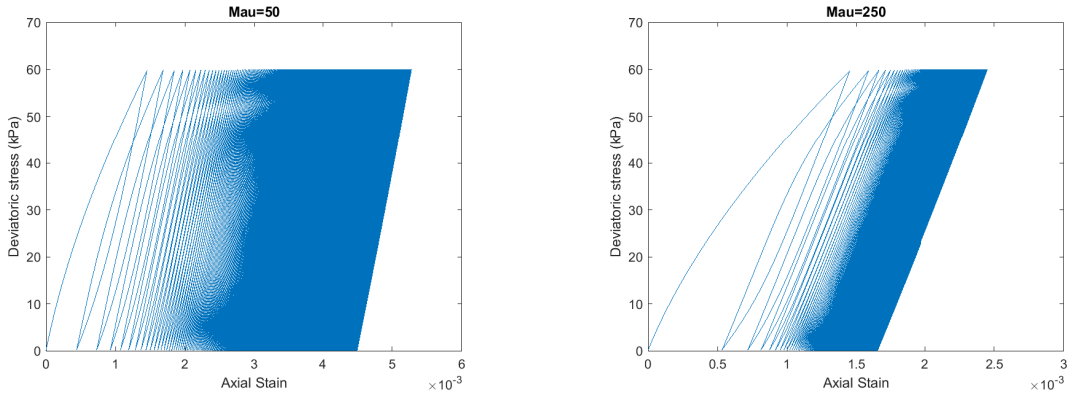

(a) $\mu = 50$ (b) $\mu = 250$

Figure 3.6: Results obtained in terms of stress-strain relationships during cyclic loading for varying memory surface parameter a) $\mu = 50$, b)$\mu = 250$

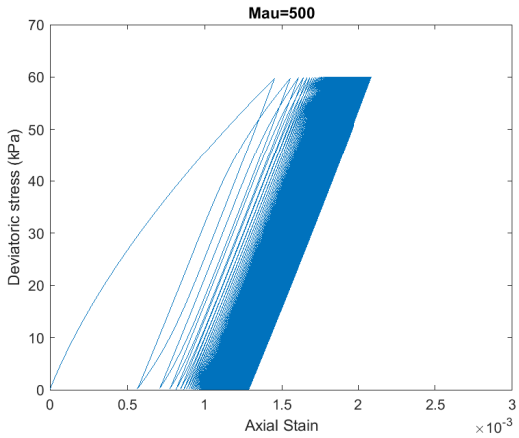

Figure 3.7: Results obtained in terms of stress-strain relationships during cyclic loading for varying memory surface parameter $\mu = 500$

When the μ value increases, gradual sand stiffening occurs and reduced plastic dissipation which can be seen with the decreasing area in the stress-strain Graph 3.6 and 3.7. With the increase in the value of M from $50 - 500$ the area tends to decrease with each cycle.

Figure 3.8 shows the change in secant stiffness and accumulated strains with the number of cycles. Higher the value of mu parameter, higher is the secant stiffness that can be illustrated through figure 3.8a. Another figure 3.8b represents the decrease in accumulated strains with the increase in mu value.

Figure 3.9 illustrates strain and stiffness rates for surface memory parameters mau and zeta. For strain rates, power equation of $f(x) = a * x^b$ is applied for curve fitting and it shows linear decrease in the strain ratcheting coefficient with the increase in mau values . Where as to determine the stiffness rate linear equation with one degree polynomial ($f(x) = p1 * ln(x) + p2$)

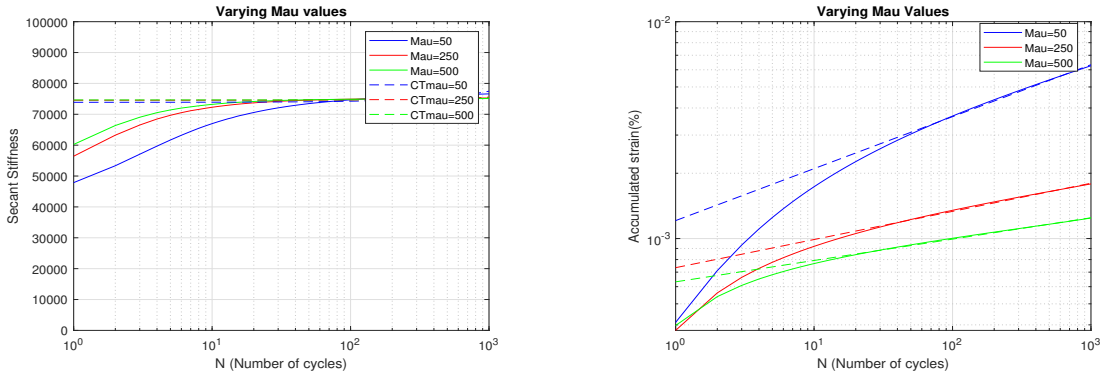

(a) Secant Stiffness (b) Accumulated Strain

Figure 3.8: a)Secant Stiffness,b)Accumulated Strain calculated from the cyclic drained loading on sands for **1000** cycles

is used. From 3.9a sudden decrease in stiffness rate but later rate becomes smooth is observed.

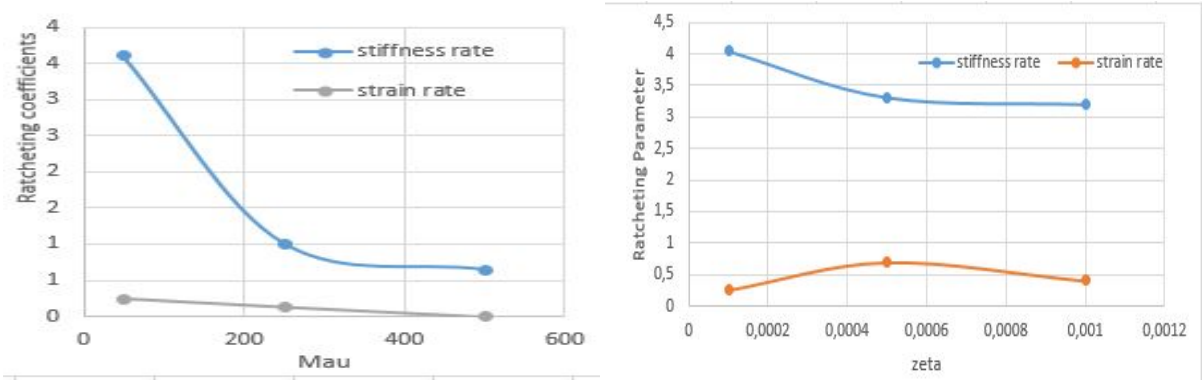

(a) Ratcheting rates (b) Ratcheting rates

Figure 3.9: Stiffness rate and strain rate calculated for memory surface parameters a)(Mau), b) (zeta)

Figure 3.10 manifests the accumulated strains and shear strains generated while cyclic loading the SANISAND MS model. Stress strain curve for shearing in figure 3.10a conveys that loop is formed with loading and unloading known as hysteresis. The area under the loop illustrates dissipated energy. This will lead to generation of irreversible shear strains. Figure 3.10b expresses, higher the mau value lesser strains will be accumulated while shearing the sand.

3.4.2. Zeta

In this part of the analysis, only zeta values are changed in the model while keeping p=100kPa, M=50, e=0.6, e=0.48, q=30kPa, q=120kPa throughout the simulation. The Stress-Strain curve, Stiffness and accumulated strains with respect to the number of cycles are observed.

Dilative behavior of sands tends to damage fabric and leads to loss of sand memory. This process can be replicated in the Sanisand MS model with the help of shrinkage of the memory surface, which is represented by the parameter (ζ) and only for dense sand as discussed above. The results 3.13, 3.12 shows that not any visual changes are observed for different zeta values while keeping other parameters the same for loose sand during cyclic loading.

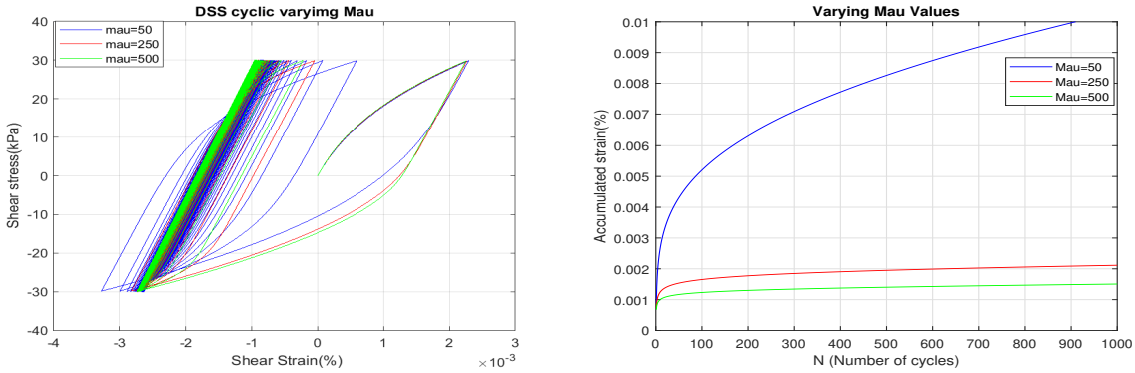

(a) Shear strains Mau (b) Accumulated strains Mau

Figure 3.10: Result obtained during drained DSS a) Shear strains Mau, b) Accumulated strains Mau

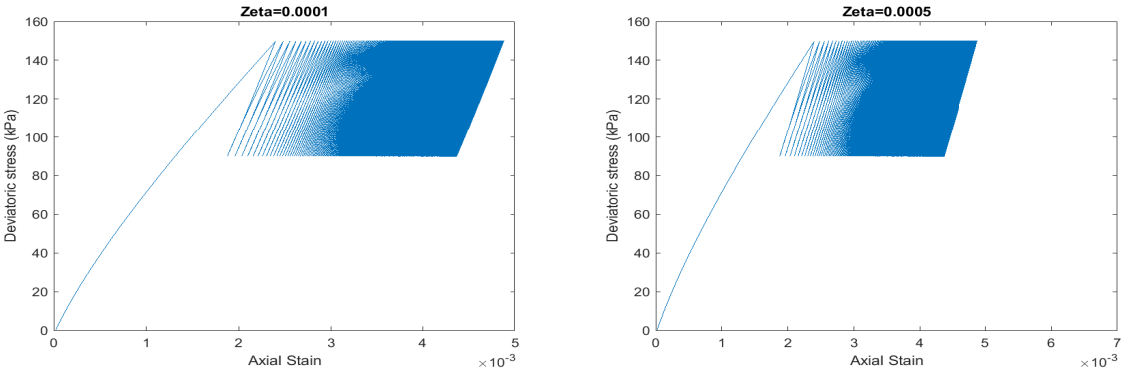

(a) Stiffness (b) Accumulated Strain

Figure 3.11: Results for varying zeta values in term of stress-strain relationship

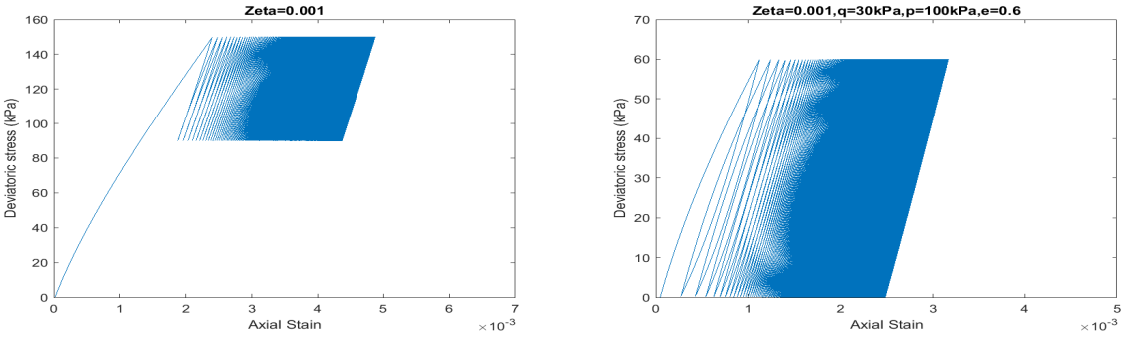

(a) Stiffness (b) Accumulated Strain

Figure 3.12: Results for varying zeta values in term of stress-strain relationship

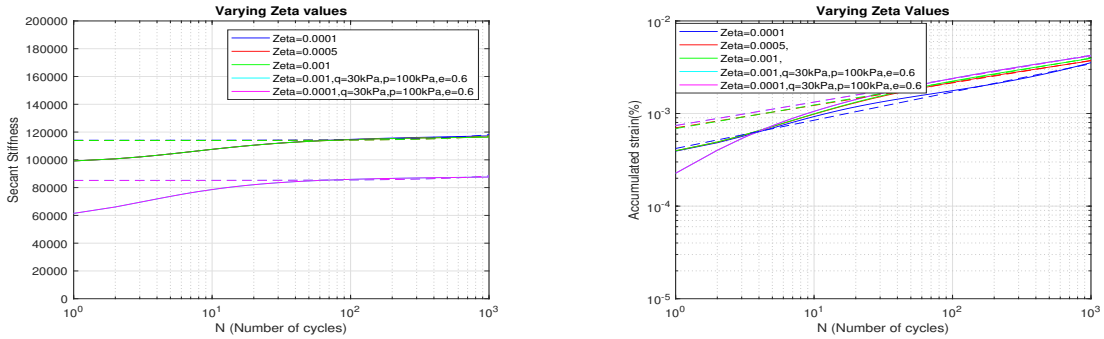

(a) Secant Stiffness (b) Accumulated Strain

Figure 3.13: Results for varying zeta values in term of a)Secant Stiffness,b)Accumulated Strain

For the ratcheting parameter, decrease can be observed in secant stiffness (3.9a) when void ratio is changed to loose sand. So denser the sand higher will be the secant stiffness. But no big changes can be observed in terms of strain accumulation while changing the void ratio from dense to loose (figure 3.13b)

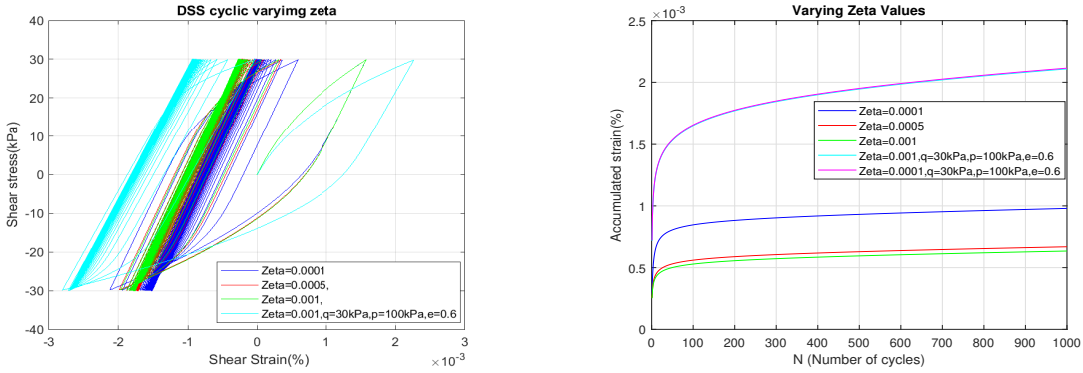

(a) Stress strain (b) Accumulated Strain

Figure 3.14: Results for varying zeta values in term of a)Stress strains,b)Accumulated Strain from drained DSS

While analysing the memory surface parameter zeta for DSS test it can be illustrated that for dense sands, less irreversible strains will be developed as compared to loose soil and also damping can be observed in figure 3.14a. Figure 3.14b illustrates for loose sand this parameter does not any change in accumulated strains but for dense sand increasing the value of zeta lesser accumulated strains are produced.

3.5. Other Parameters

3.5.1. Void Ratio(e)

Sanisand MS model has been analysed to observe the influence of the void ratio in the sand under drained triaxial loading. The parameters taken for this analysis are zeta=0.001,mu=50, p=100kPa, q=30kPa, e=0.6,0.7,0.8.

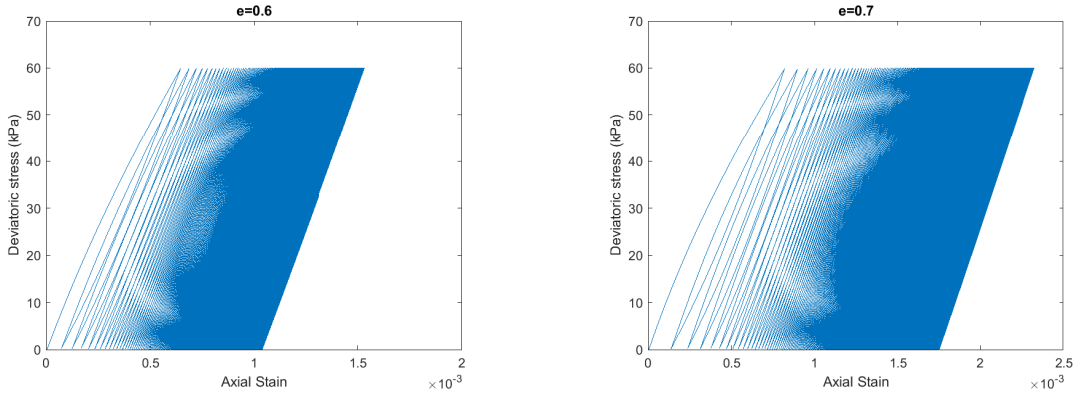

(a) e=0.6 (b) e=0.7

Figure 3.15: Results for varying void ratio in term of stress-strain graph for a)e=0.6, b)e=0.7

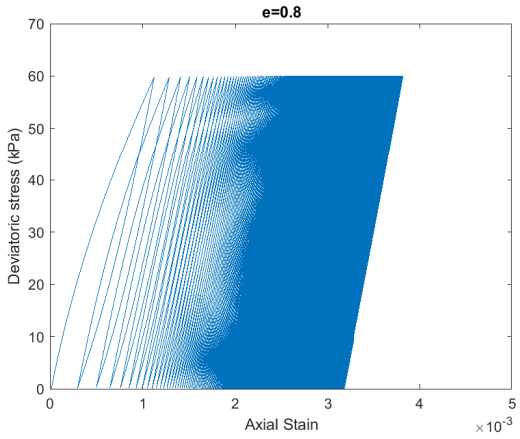

Figure 3.16: Results for varying void ratio in term of stress-strain graph for e=0.8

The influence of deviatoric stress with respect to axial strain is illustrated in 3.15 for varying void ratios. With the increase in void ratio or soil becoming loose, there is a shift in the axial strains and an increase in the area under the stress-strain is observed.

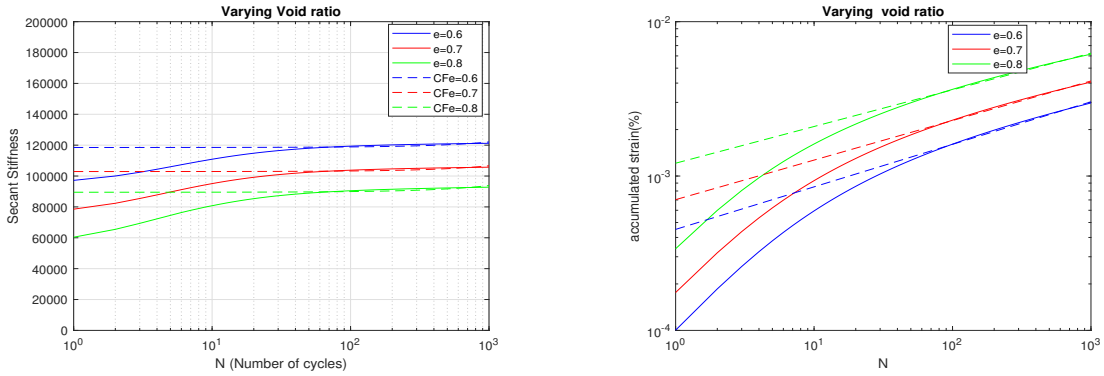

(a) Secant Stiffness

(b) Accumulated Strain

Figure 3.17: Results for varying void ratio in term of a)Secant Stiffness,b)Accumulated Strain for **1000** loading cycles

Figure 3.17a shows loser the sand, lesser will be the secant stiffness through out 1000 cycle. Also higher will be strain accumulated while applying triaxial loading. Stiffness rate and strain rate are calibrated using power law equation and are illustrated in figure 3.18. It can be observed that strain rate tends to remain same but stiffness rate increases with the increase in void ratio.

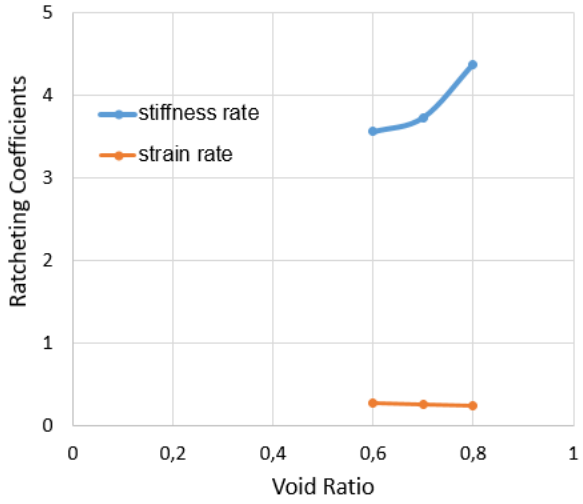

Figure 3.18: Ratcheting rate for varying Void ratio

3.5.2. Deviatoric Stress/ average stress(q_d)

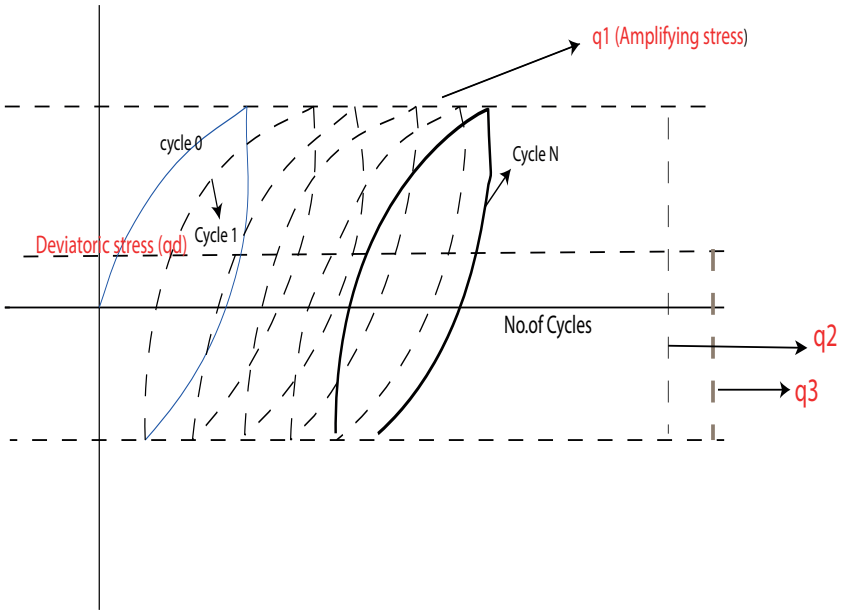

Figure 3.19: Definition of deviatoric stress (qd) and amplitude stress (q1)

Figure 3.19 explains the definition of deviatoric/ average stress q_d and amplifying stress q_1 with respect to number of cycles. Amplifying stress q_1 is always equal to q_3 and q_2 needs to be double of q_1 in the analysis.

Analysis for Deviatoric stress is done for 30kPa, 60kPa, 90kPa while the other parameters are kept constant e= 0.7, zeta=0.0001, mu=50, p=100kPa. The Stress-Strain relationship below shows with the increase in the deviatoric stress on the loose sand sample, the axial strains keeps on increasing.

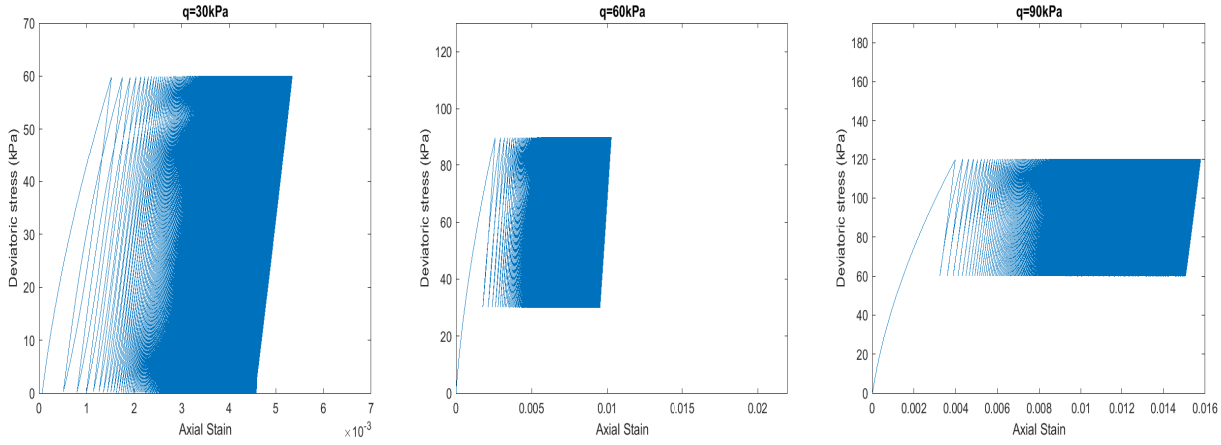

(a) qd=30kPa (b) qd=60kPa (c) qd=90kPa

Figure 3.20: Results for varying deviatoric stress in term of stress-strain graph a)qd=30kPa, b)qd=60kPa, c)qd=90kPa

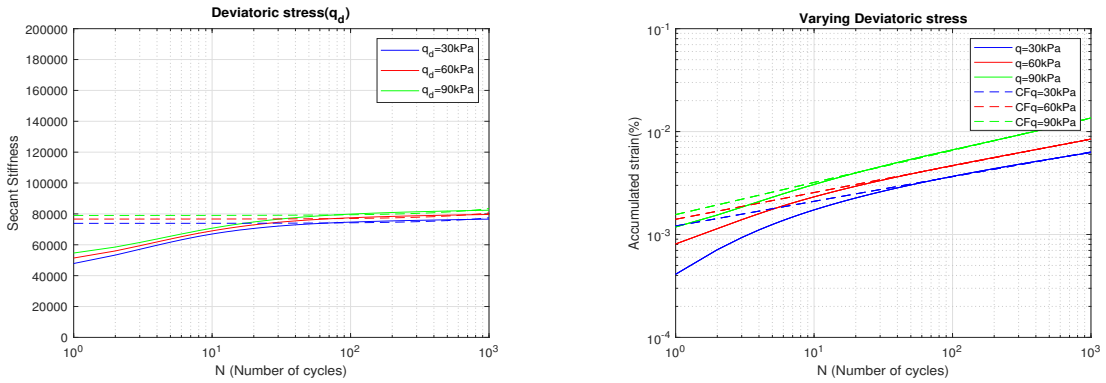

(a) Shear Stiffness (b) Accumulated Strain

Figure 3.21: Results for varying deviatoric stress in term of a)Secant Stiffness,b)Accumulated Strain

From the 3.21 Accumulated strains rate tends to remain same with the increase in the number of cycles .And from 3.22, higher the deviatoric stress, higher would be the stiffness up to 10-15 cycles but with further cyclic loading, stiffness would become linear and stagnant. Figure 3.22 illustrates no change in strain rates whereas stiffness rate increases linearly with increasing deviatoric stress.

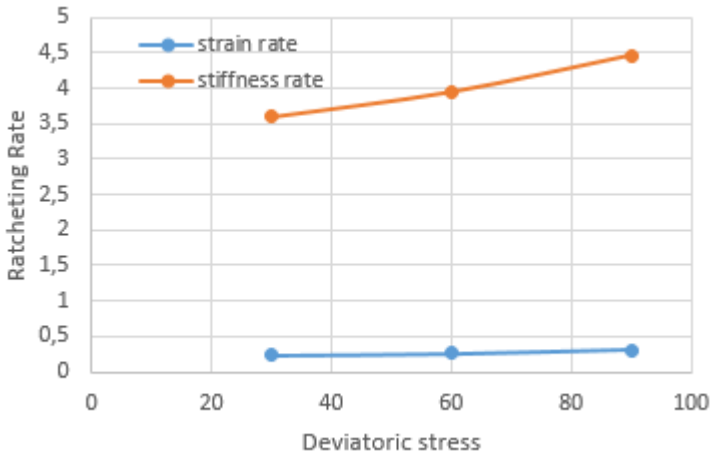

Figure 3.22: Results for varying deviatoric stress in term of Ratcheting rate

3.5.3. Amplitude stress(q1)

Analysis of the amplitude stress is done for q_1 $30kPa, 45kPa, 60kPa$. Other parameters zeta, mau, deviatoric stress, confining stress are kept constant during this analysis.

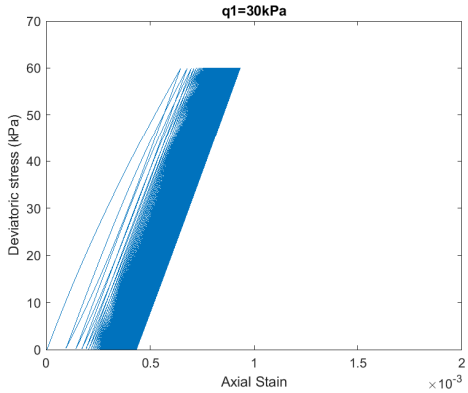

(a) q1=30kPa

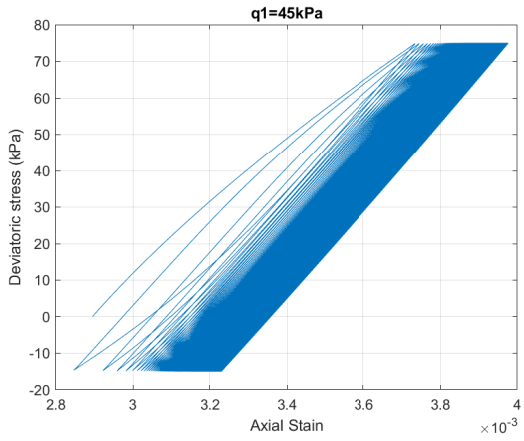

(b) q1=45kPa

Figure 3.23: Results for varying amplitude stress in term of stress- strain graph a)q1=30kPa, b) q1=45kPa

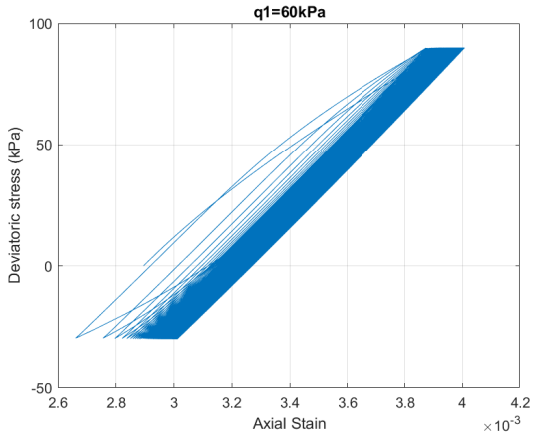

Figure 3.24: Results for varying amplitude stress in term of stress- strain graph q1=60kPa

3.25b shows, increase in the accumulated strains with the increase in the stress level. 3.25a the stiffness remains constant, showing no effect of stress levels. Vaguely any changes in both strain and stiffness rate can be seen in figure 3.26.

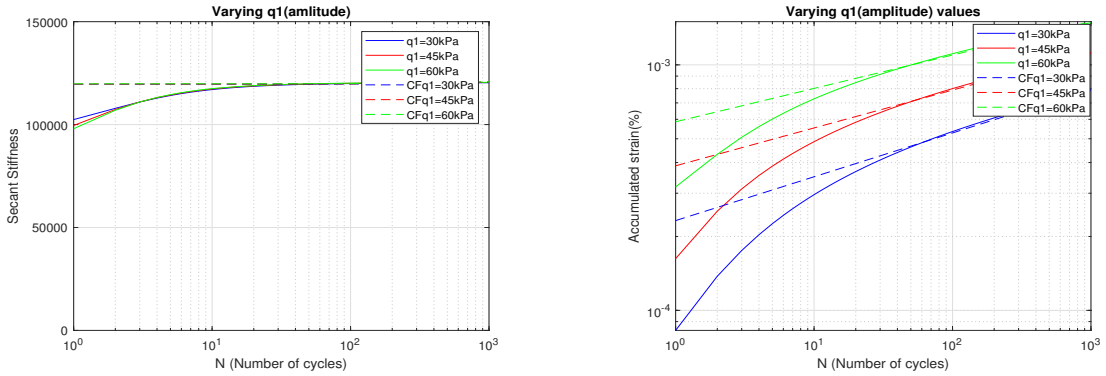

(a) Secant Stiffness (b) Accumulated Strain

Figure 3.25: Results for varying amplitude stress in term of a)Accumulated Strain,b)Secant Stiffness

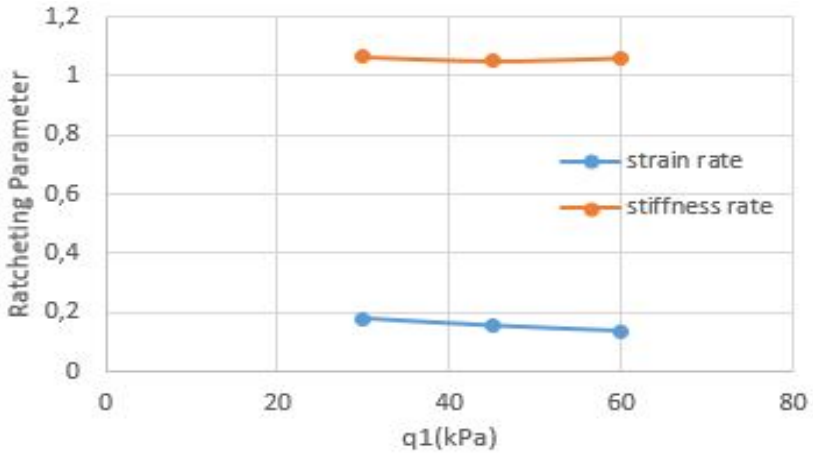

Figure 3.26: Results for varying amplitude stress in term of Ratcheting rate

3.5.4. Confining Pressure (p)

3.27 and 3.29 illustrate the influence of confining pressure on the strains, total accumulated strains, and stiffness. The increase in confining pressure shows the decrease in the area under the stress-strain curve. Total accumulated strains decrease with the increase in the confining pressures. But the contrast of strains can be seen in stiffness, as stiffness increases with confining pressure. The Ratcheting rates graph 3.30 shows both ratcheting rate for stiffness and strain increases.

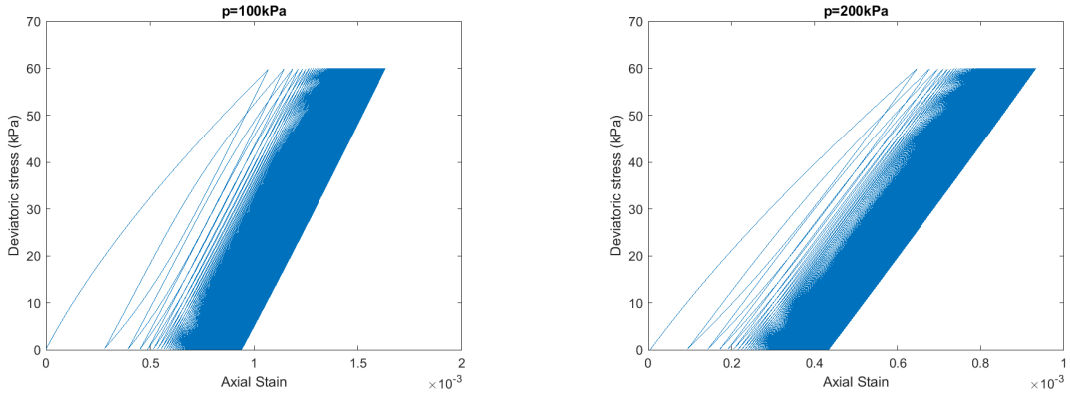

(a) p=100kPa (b) p=200kPa

Figure 3.27: Stress- strain graph for varying confining pressures a) p=100kPa, b)p=200kPa

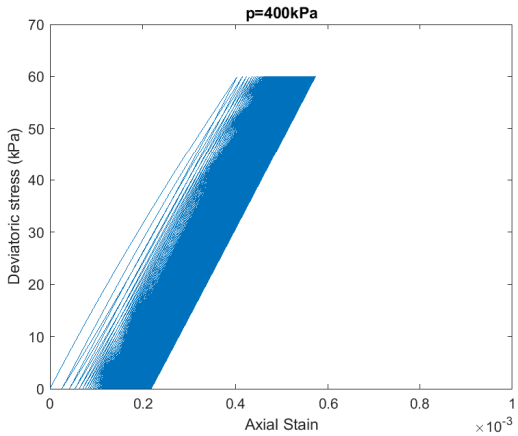

Figure 3.28: Stress- strain graph for varying confining pressures p=400kPa

3.5.5. Strain Superposition

Superposition method aids to predict the varying amplitude lateral cyclic loads applied to the piles. With the already known strains developed during cyclic loading of deviatoric stress and amplitude stress, multiple cyclic strains can be predicted. Figure 3.31 is used to explain the process of superposition application on loads. For the first 500 cycles, from curve 1 strain level is determined (A). Numerically this curve could be draw using equation 5.5. The strain level equivalent to A is searched on curve 2. This will predict the strains for next 500 load cycles using equation 5.6. The strains from the previous cycle1 are superimposed on cycle2. This method is applicable for only successive load levels. It is valid for 50 cycles and more.

$$y_1 = a_1 * N_1^{b_1} \tag{3.19}$$

$$y_2 = a_2 * (N_{12} + N_2)^{b_2} \tag{3.20}$$

Figure 3.32 illustrates the strain superposition applied to Deviatoric stress in graph 3.32a and for amplitude stress in 3.32b. In incremental order of loading, this method could be helpful to estimate the accumulated strain. But detrimental loading, it overestimates the strains since superposition leads to addition of previous load with each step.

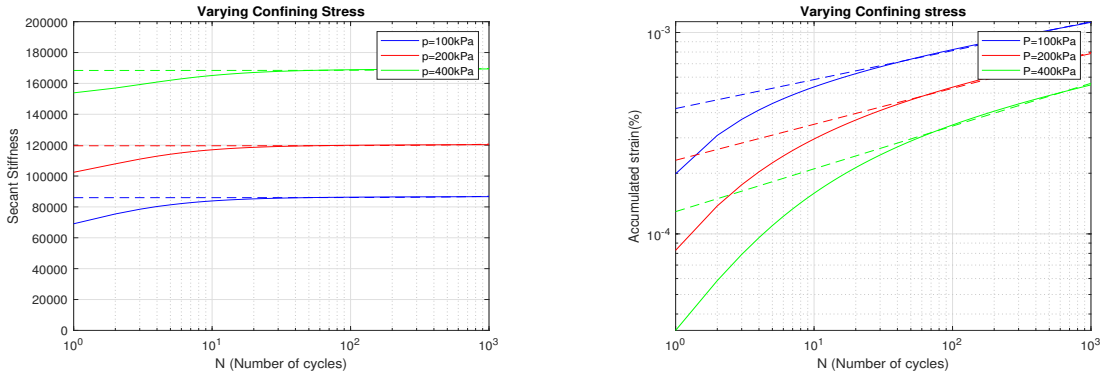

(a) Stiffness (b) Accumulated Strain

Figure 3.29: Results for varying confining pressures a)Accumulated Strain, b)Secant Stiffness

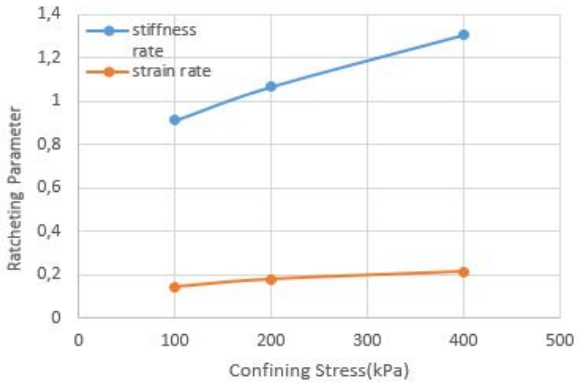

Figure 3.30: Results for varying confining pressures as Ratcheting rate

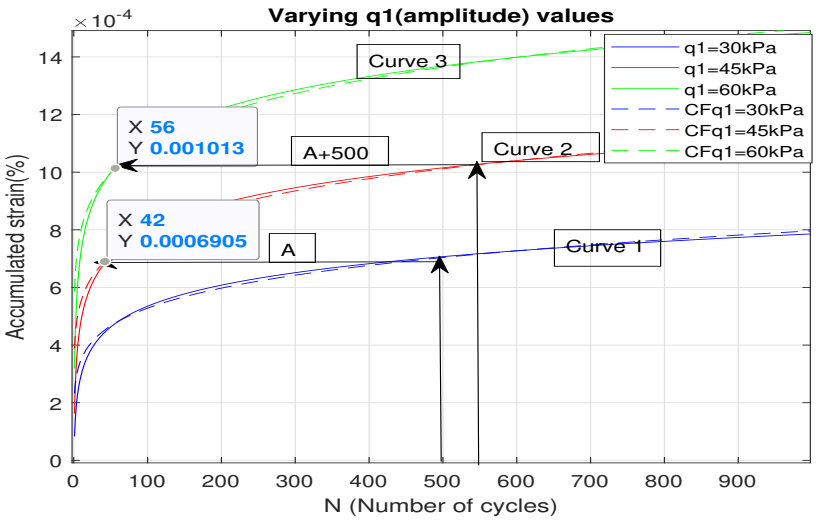

Figure 3.31: Method used for predicting pile permanent displacement for mixed loading

3.5.6. Multi amplitude cyclic loading

1. Deviatoric Stress

Monopile is subjected to varying cyclic loading. The strains developed in the loose sand from multiple cyclic loading with 500 cycles and varying amplitude load series are plotted

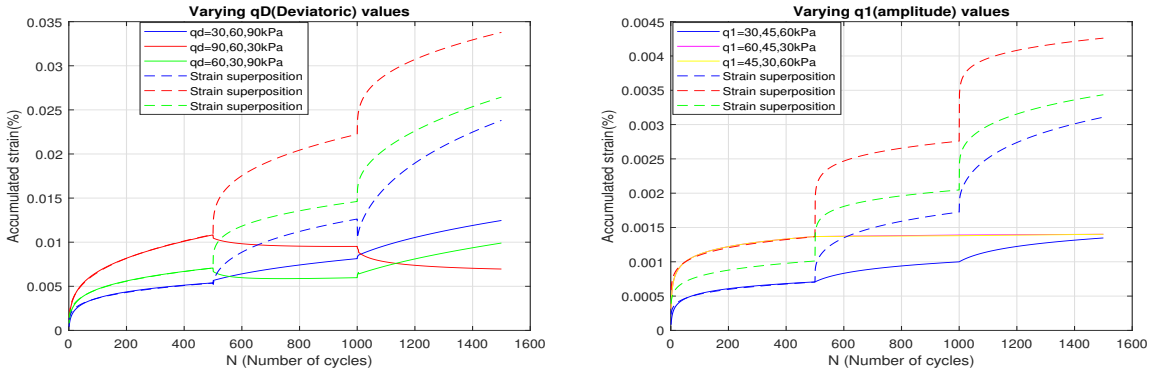

(a) Strain superposition qd

(b) Strain superposition q1

Figure 3.32: Accumulated strains predicted using Strain superposition for a) Deviatoric stress, b) amplitude stress and compared with actual mixed loads strains

No.	p(kPa)	μ	ζ	e	q_d(1,2,3)(kPa)	q_1(1,2,3)(kPa)	Cycles
1	100	50	0.0001	0.7	30,60,90	30,30,30	500
2	100	50	0.0001	0.7	90,30,60	30,30,30	500
3	100	50	0.0001	0.7	60,30,90	30,30,30	500
4	200	250	0.001	0.6	30,30,30,	30,45,60	500
5	200	250	0.001	0.6	30,30,30	60,30,45	500
6	200	250	0.001	0.6	30,30,30	60,45,30	500

Table 3.2: Numerical study program for Multiple cyclic loading

in fig 3.34. These series of load cycles explores about the effects of load histories in the order they are applied.

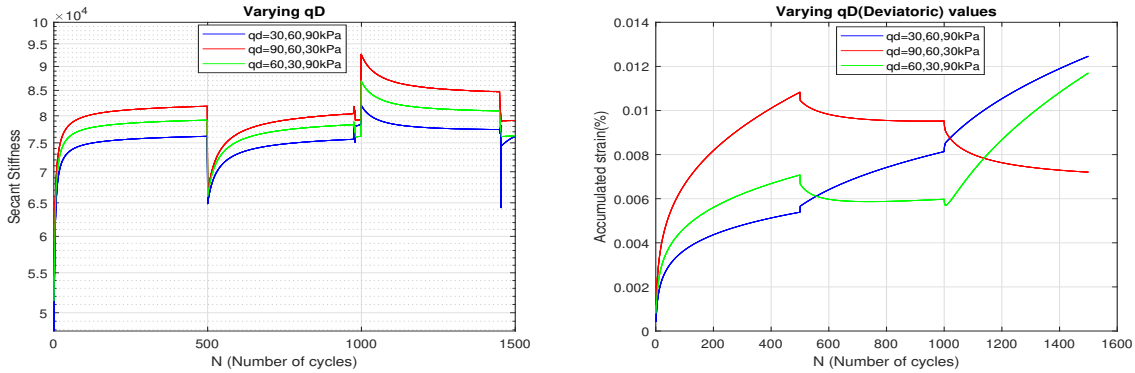

(a) Secant stiffness

(b) Accumulated strain

Figure 3.33: Results for multiple cyclic loading with varying deviatoric stress a)Secant stiffness, b)Accumulated strain

Figure 3.33b illustrates the accumulated strains with respect to three cyclic loading tests. As a result this graph conveys marginal change in the final strains with each load cycle. Figure 3.33a shows secant stiffness with respect to number of cycles. It can be concluded that larger the load history before the next cycle, stiffer is the response. That is why secant stiffness of (qd=90,60,30kPa)> (qd=60,30,90kPa)>(qd=30,60,90kPa).

2. Amplitude Stress(q1) Frame work of load cycles is applied to varying amplitude stresses.

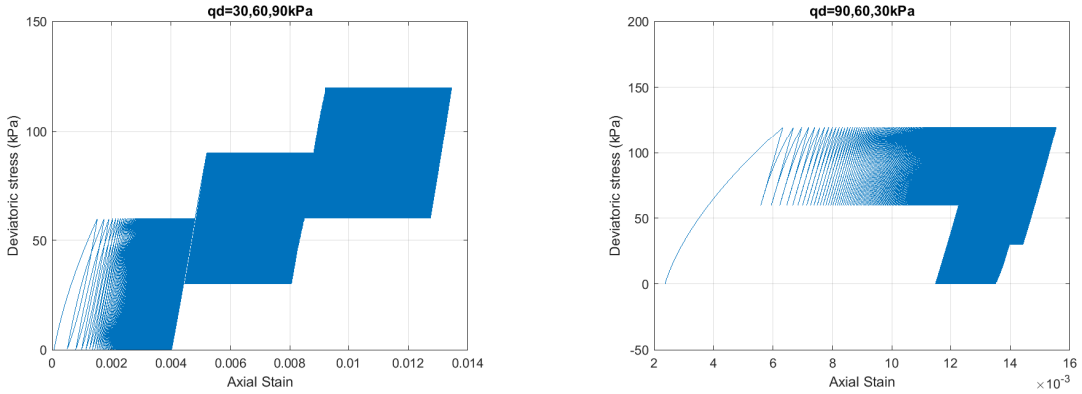

(a) qd=30,60,90kPa (b) qd=90,60,30kPa

Figure 3.34: Results for mixed loading with varying deviatoric stress as Stress-Strain relationship

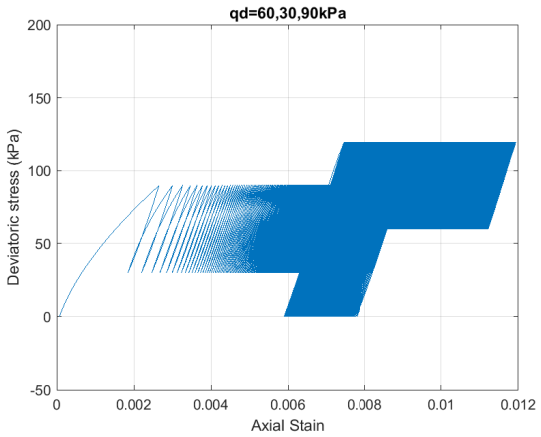

Figure 3.35: Results for mixed loading with varying deviatoric stress as Stress-Strain relationship

Figure 3.37 illustrates the stress- strain relationship when varying amplitude stresses are applied. Figure 3.36b illustrates the accumulated strains with respect to three cyclic

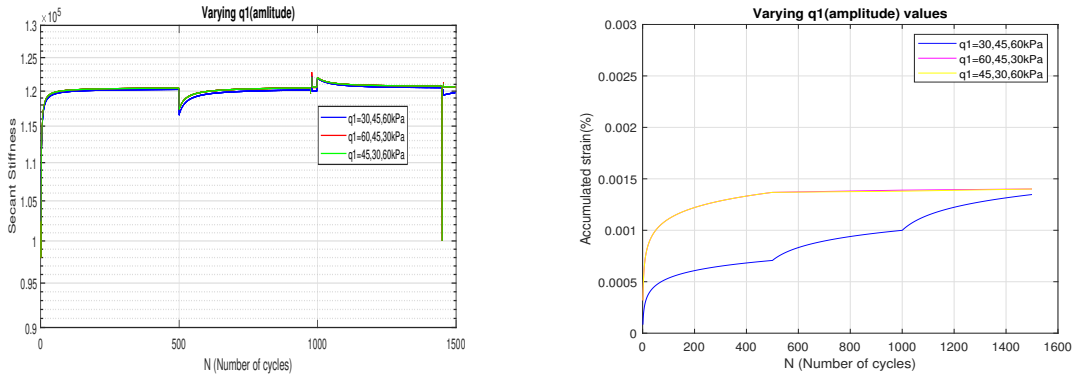

(a) Secant stiffness (b) Accumulated strain

Figure 3.36: Results for mixed loading with varying amplitude stress as a) Secant stiffness, b) Accumulated strain

loading's. As a result this graph conveys marginal change in the final strains with each load cycle. But interesting thing to observe in graph 3.36a is that secant stiffness is similar

for all loading sequences (q1=30,45,60kPa)= (q1=45,30,60kPa)=(q1=60,45,30kPa).

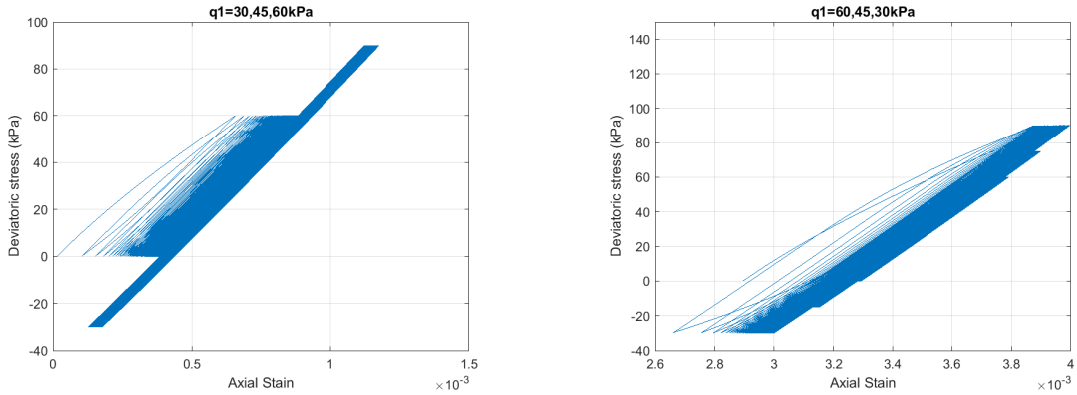

(a) q1=30,45,60kPa (b) q1=60,45,30kPa

Figure 3.37: Results for mixed loading with varying amplitude stress as Stress-Strain relationship

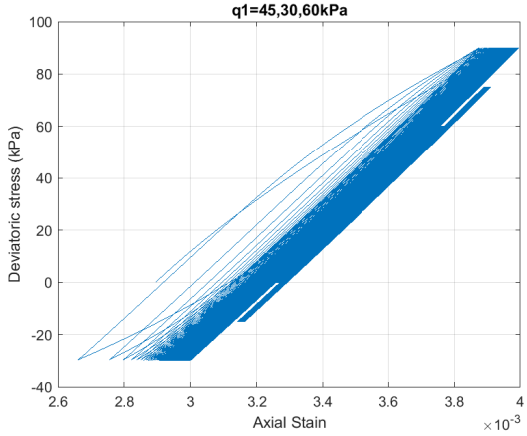

Figure 3.38: Results for mixed loading with varying amplitude stress as Stress-Strain relationship (q1=45,30,60kPa)

3.6. Summary

1. SANISAND-MS model is able to predict the sand behavior under different pressure and void ratio with single set of parameters.
2. Memory surface theory is able to capture the cyclic sand behavior. The accumulated strain rate decreases with increase in the number of cycle, while secant stiffness increases.
3. The influence of void ratio, initial confining pressure and memory surface parameters are investigated on the ratcheting behavior of sand.
4. The loading sequence of a series of load parcels is investigated and miner rule-based superposition method is found to be suitable when the load parcels as in ascending order.
5. For deviatoric stress, it can be concluded that if the previous load is higher, the accumulated strain at the next loading will decrease.
6. During Multiple cyclic loading, secant stiffness remains same for all sequences of loading for amplifying stresses.

4

3D FE modelling of monopile subjected to lateral loading

4.0.1. Introduction

Since the OWT would be subjected to strong cyclic loading originating from wind or waves throughout the lifetime, affecting the ultimate strength of the structure. Aspects that need to be considered while designing offshore wind turbine foundations are deformation and stiffness. Long-term cyclic loading also changes the interaction between the pile and the soil leading to rotation. It is possible to create a prototype to study the behavior between pile and soil during loading, but that will be time-consuming and expensive [44], [20]. An advanced 3D finite element (FE) modelling for the dynamic analysis of OWT-monopile-soil is set up for accounting for dynamic soil-monopile interaction in presence under cyclic loading [25],[24]. Instead, a model of pile soil is set up in the OPENSEES platform to determine the strains and displacements generated in the piles under high cyclic ratcheting[11], [16]. It uses the programming language of tcl, and C++. The Open System for Earthquake Engineering Simulation is a software framework developed to stimulate research in the seismic response of structural and geo-technical systems during earthquakes. It provides a wide range of material models, elements, and solution algorithms for modeling and analyzing the nonlinear response of systems. The software can also be helpful for parallel computing to allow scalable simulations on high-end computers or for parameter studies. Finite element model has been created for pile1 and its pictorial representation is Fig. 4.1.

The model shows Fig.4.1 a circular steel pipe pile with a length L $20m$, a diameter D $5m$, a thickness t $0.1m$, and an eccentricity ratio (e/L) 1 in the center, and surrounded by the sand. For better efficiency, only half the domain has been modeled. The size of the domain is $65.1m, 32.5m, 30m$, and it has meshed inconsistently. Meshes next to the pile are dense whereas far away are loosely meshed. The bottom, side boundaries for the model are fixed, implying no displacement possible but the top is free. Both soil and embedded pile is discretised below the mother line as solid element with 8 nodes and above mother line pile is discretized as beam element. Firstly, gravity load is applied in the model to compensate for installation effects. In later steps, lateral monotonic ($0.1D$) and cyclic loading is applied. Finite element modeling software OPENSEES PL is used for setting boundaries and meshing the whole model.

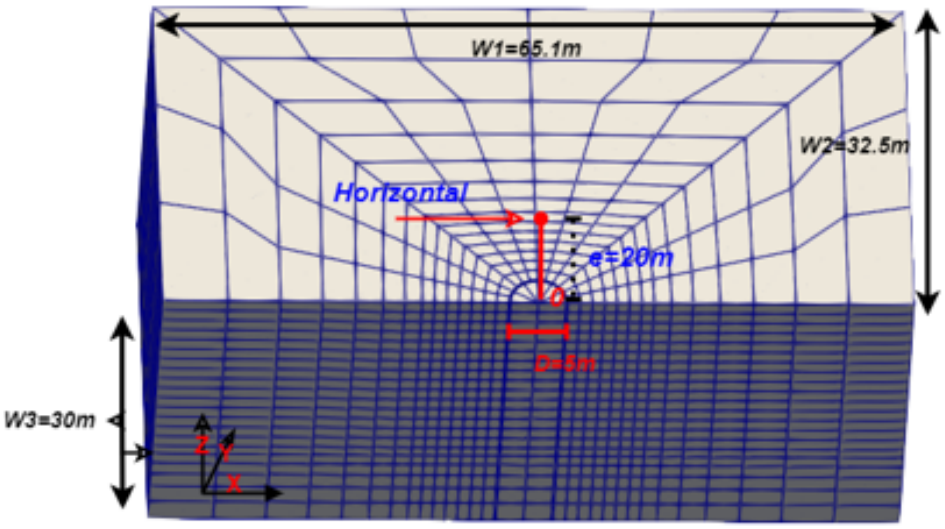

Figure 4.1: FE model domain with pile soil discretization

4.1. Monotonic loading

A stiff model monopile is subjected to the monotonic lateral load. A set of 11 test have been prepared table. 4.1. These pile test had been done to study the influence of the length,diameter,thickness and eccentricity on the displacement and rotation.

4.1.1. Simulation Plan

Table 4.1: Numerical simulation program to study of effect of pile geometry during Monotonic Loading

No.	L(m)	D (m)	Int.Dia(m)	Thickness(m)	Eccentricity(h/L)	H.force at 2degree
1	20	5	4,8	0,1	1	12580
2	20	5	4,7	0,15	1	13190
3	20	5	4,6	0,2	1	13330
4	20	6	5,6	0,2	1	15960
5	20	10	9,6	0,2	1	28840
6	20	8	7,6	0,2	0,5	31050
7	20	8	7,6	0,2	1	21920
8	20	8	7,6	0,2	1,5	16920
9	20	6	5,6	0,2	1,2	14287
10	25	6	5,6	0,2	1,2	19492
11	30	6	5,6	0,2	1,2	27603

4.1.2. Pile Geometry effect

Figure 4.2 and 4.3 illustrates rotation in pile while applying laterally loading depending upto varying pile geometry. These graphs are plotted between horizontal forces and pile rotation. Graph 4.2a shows no considerable effect of pile thickness on pile rotation. From graph 4.2band 4.3b demonstrates increasing the diameter or length, higher lateral forces are needed to achieve the desired rotation in the pile. Graph 4.3a shows with the increase in eccentricity length lesser force will be required for rotation. To limit the rotation of the monopile to smaller than 0.5 degree, (DNV) throughout the serviceability life of OWT for safer operations, the pile rotation

of 2 degrees is chosen as a reference index to determine cyclic load by Leblanc.

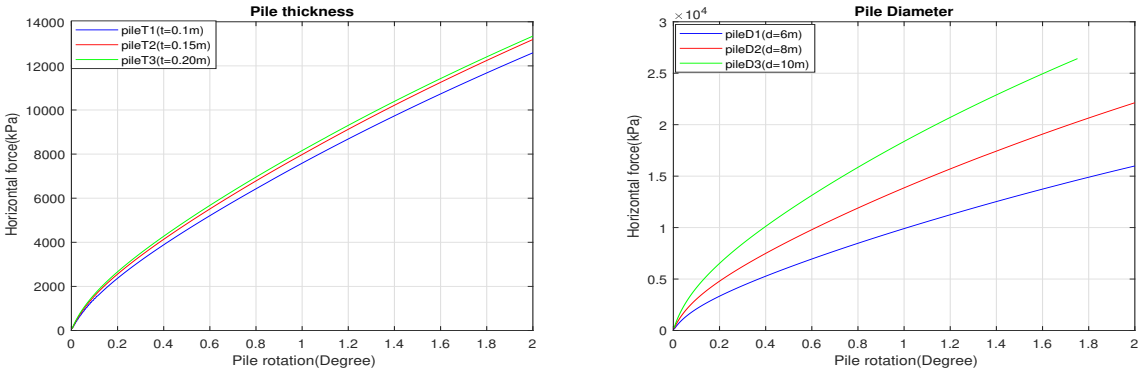

(a) Pile thickness (b) Diameter

Figure 4.2: Pile rotation obtained during lateral monotonic loading on FE model for different pile geometries a)pile thickness, b) diameter

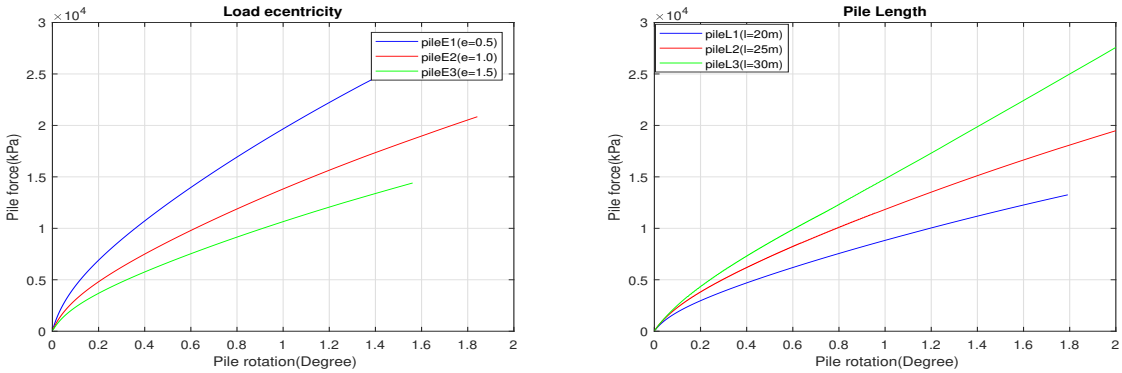

(a) Load eccentricity (b) Pile length

Figure 4.3: Pile rotation obtained during lateral monotonic loading on FE model for different pile geometries a) Pile length, b)load eccentricity

To provide a better understanding of the lateral loads on the monopiles and to make these data more reliable for other pile dimensions, data is converted to a dimensionless / normalization method. Two different schemes used here to do so are Moment-Pile rotation4.4 and Load-displacement 4.5. Pile forces at 2-degree rotation are chosen as references for cyclic loading. Equation 2.7 and 2.4 has been adopted to visualize figure 4.4. All four pile geometry parameters (Length, Diameter, Load eccentricity, and thickness) are addressed together in this graph with different trend lines.

Another formulation of the normalization has been used in the figure 4.5 by Achmus. For the normalization purpose the equation 4.1 is applied. Each trend line shows the influence of the parameter on the lateral displacement during incremental load applied to the pile.

$$\tilde{H} = \frac{H(h+L)}{L^3 D \gamma_s'} \tag{4.1}$$

4.1.3. Soil response under lateral monotonic load

While subjecting the pile through lateral monotonic loading, a change in relative density is expected. Figure 4.6 illustrates the densification and loosening of soil around the pile. Loading

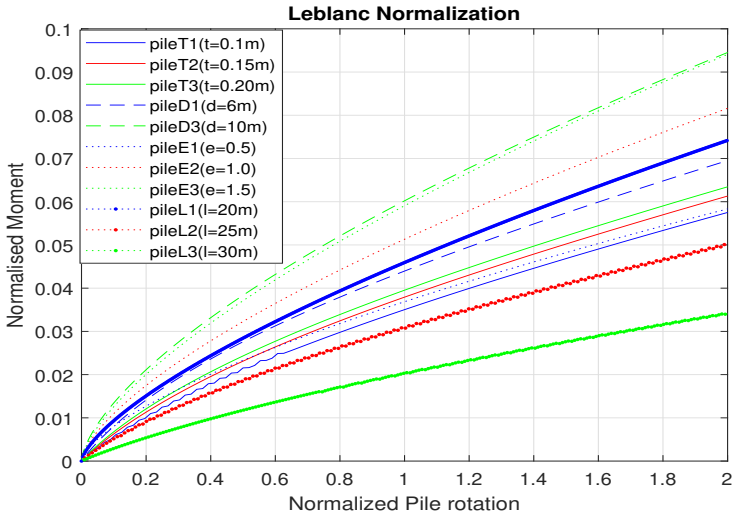

Figure 4.4: Pile rotation calculated using FEM for different pile geometries while normalizing moment and rotations through Leblanc Normalized formulation

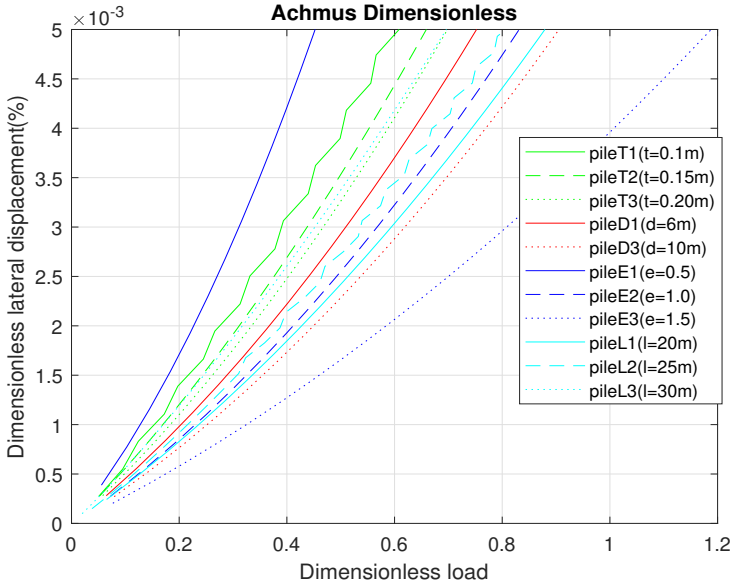

Figure 4.5: Pile rotation calculated using FEM for different pile geometries while normalizing moment and rotation Achmus formulation

in the x-direction, soil's relative density increases in the direction of force, whereas decreases on the opposite side till the neutral axis. At the bottom, part soil loosens in the direction of loading and densifies at the other. From the figure, it can be stated that lateral forces try to rotate the pile in the direction of loading.

Figure 4.7 illustrates the magnitude of displacement developed during monotonic loading of the pile. Deformation of the meshing shows that due to lateral load in x direction the whole profile along with pile will try to move along causing tilt in the pile. Most of the displacements will take place around the pile head and later will deteriorate along the pile length.

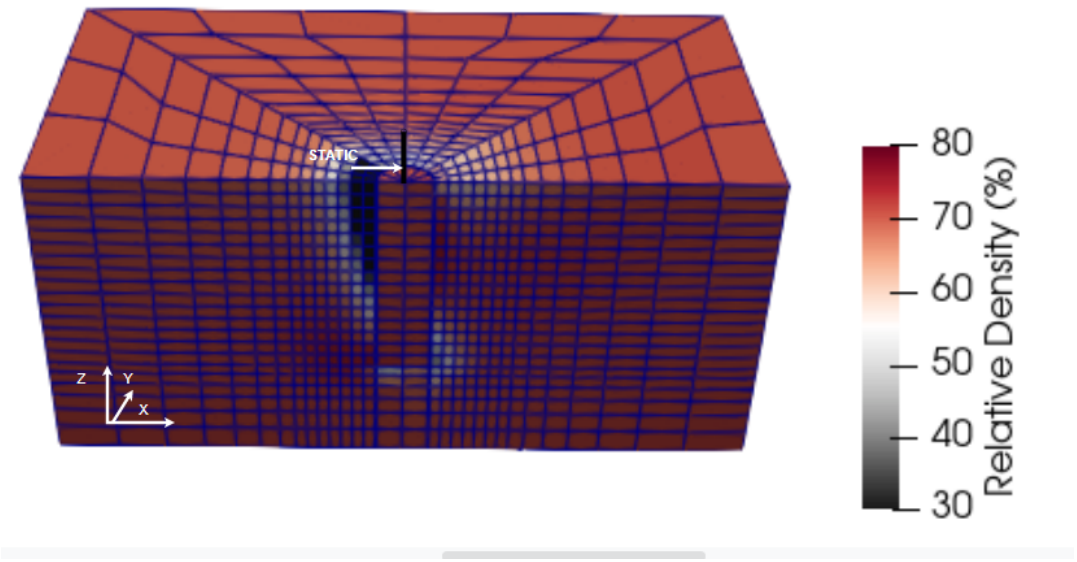

Figure 4.6: Change in relative density of sand during lateral monotonic loading applied in FEM

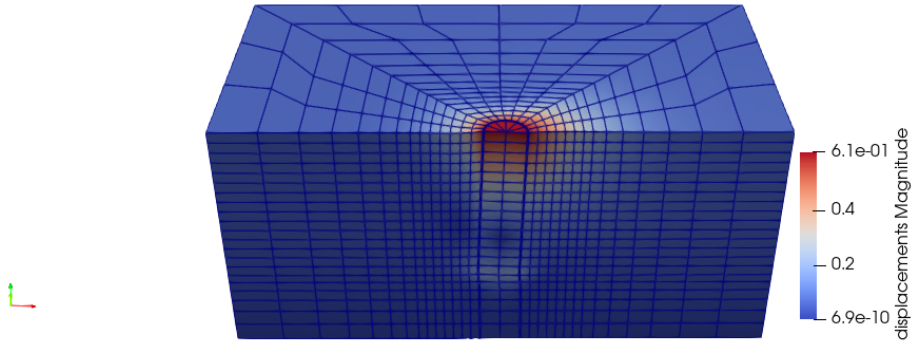

Figure 4.7: Visualization of tilting occurring in pile during lateral monotonic loading applied in FEM

4.2. Cyclic Loading

Irregular winds and waves leads to the cyclic loading on the offshore structures. These loading tends to generate rotations and deformation into the monopiles. In order to study the effect of cyclic loading on monopiles, a set of 12 pile tests have been done. Table 4.2 discovers influences of pile length, diameter, load eccentricity,and Memory surface parameters (μ,ξ).

4.2.1. Pile Geometry effect

Figure 4.8a shows the effect of monopile diameter (d=6m, d=8m, d=10m) during cyclic loading . Lines in the graph illustrate accumulated rotation in the pile due to generation of irreversible plastic strains (ratcheting). Increasing the pile diameter shows similar rotations of the pile.

Figure 4.8b displays the end results of the monopile length (L=20m, 25m, 30m) during 100 loading cycles with constant amplitude in terms of normalized rotations. Results conclude that with the increase in the pile length the rotations would be less.

Graph 4.9 illustrates rotations developed in piles with the number of cycles with the effect of the variation in the moment arm(h) or load eccentricity. From this graph it can be noted that the moment arm to which lateral load is being applied does not show a much difference in the

Table 4.2: Numerical simulation programme to study effects of varying pile geometries and memory surface parameters while Cyclic Loading

Pile	1	2	3	4	5	6	7	8	9	10	11	12
Geometry												
Diameter	6	10	6	6	6	8	8	8	6	6	6	6
Length	20	20	20	25	30	20	20	20	20	20	20	20
Load eccentricity	1	1	1,2	1,2	1,2	0,5	1	1,5	1	1	1	1
Cyclic LF												
eta b	0,1	0,1	0,1	0,1	0,1	0,1	0,1	0,1	0,1	0,1	0,1	0,1
eta c	0	0	0	0	0	0	0	0	0	0	0	0
Memory F												
mau	200	200	200	200	200	200	200	200	100	300	200	200
zeta	0,0005	0,0005	0,0005	0,0005	0,0005	0,0005	0,0005	0,0005	0,0005	0,0005	0,001	0,0001
F(ref)	15960	28840	14287	19492	27603	31050	21920	16920	15960	15960	15960	15960

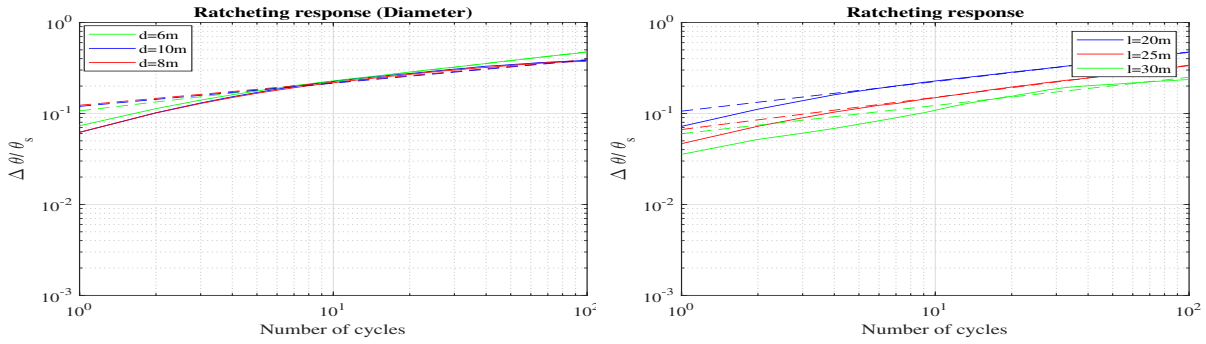

(a) Ratcheting response (Diameter)

(b) Ratcheting response (Length)

Figure 4.8: Ratcheting response (Rotation) calculated for different pile geometries (a) Diameter, (b) Length during lateral cyclic loading

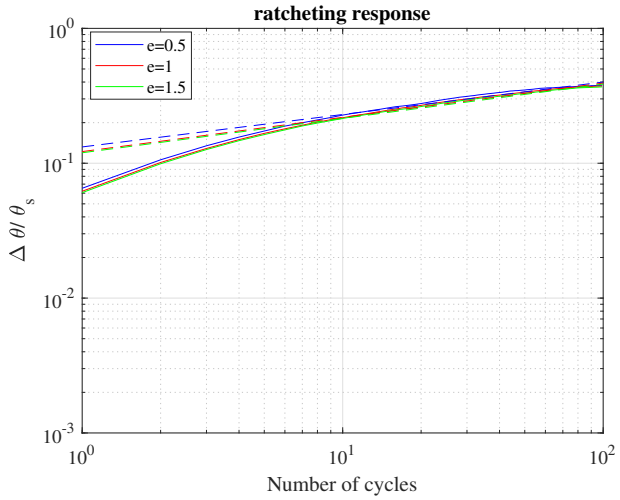

Figure 4.9: Ratcheting response (rotation) calculated for different pile geometries (Load eccentricity) during lateral cyclic loading

rotation of the pile with 100 cycles. The plastic strains leading to ratcheting develop a similar amount of rotations with increase in moment arm length.

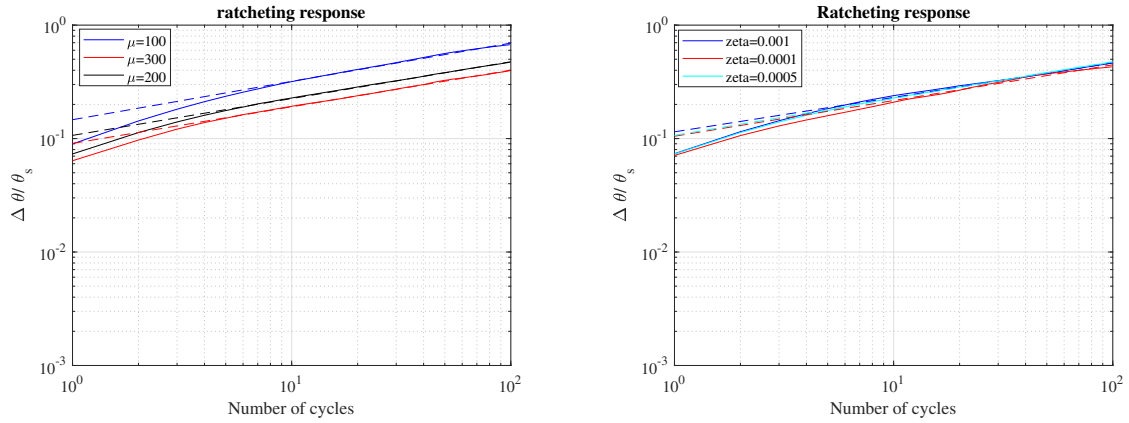

(a) Ratcheting response (μ)

(b) Ratcheting response (ξ)

Figure 4.10: Ratcheting response of model under drained cyclic loading while varying Memory surface parameters a) (μ), b)(ξ)

4.2.2. The effect of Memory Surface Parameters

μ and ξ are the parameters of the memory surface in SANISAND MS model. The expansion of the memory surface captures the phenomenon of sand stiffening and change in fabric. This occurs due to the reduced plastic strain dissipation during loading. From the graph 4.10a it can be concluded that with the increase in the μ value less rotations will be developed in piles.

Dilative behavior which damages the fabric and tends to erase the sand memory is represented with the ξ. With the change in value of ξ, a notable change in the rotation of the pile can not be observed. Loose drained sand condition is opted for the analysis. That is why ξ does show a minute effect in the rotation of the pile.

4.2.3. Loading Factor

ζ_b ,ζ_c can be defined as the loading factor coefficients. These coefficients were introduced firstly by [28] to predict the accumulated rotation due to loading characteristics. A set of 19 tests has been taken into account to study rotation accumulation due to loading factors.

Table 4.3: Numerical simulation program for varying pile geometries and memory surface parameters corresponding to Tb-Tc values

	1	2	3	4	5	6	7	8	9	10	11	12	14	15	16	17	18	19
Geometry																		
Diameter	6	6	6	6	6	6	8	8	8	8	8	8	6	6	6	6	6	6
Length	30	30	30	30	30	30	20	20	20	20	20	20	20	20	20	20	20	20
Load eccentricity	1,2	1,2	1,2	1,2	1,2	1,2	1	1	1	1	1	1	1	1	1	1	1	1
Cyclic LF																		
eta b	0,1	0,2	0,3	0,1	0,1	0,1	0,1	0,2	0,3	0,1	0,1	0,1	0,2	0,3	0,1	0,1	0,1	0,1
eta c	0	0	0	-0,75	-0,5	0,5	0	0	0	-0,75	-0,5	0,5	0	0	-0,75	-0,5	0	0,5
Memory F																		
mau	200	200	200	200	200	200	200	200	200	200	200	200	200	200	200	200	200	200
zeta	0,0005	0,0005	0,0005	0,0005	0,0005	0,0005	0,0005	0,0005	0,0005	0,0005	0,0005	0,0005	0,0005	0,0005	0,0005	0,0005	0,0005	0,0005
F(ref)	27603	27603	27603	27603	27603	27603	21920	21920	21920	21920	21920	21920	15960	15960	15960	15960	15960	15960

Value of ζ_b can vary from 0 to 1 telling about the magnitude of loading measuring the size of cyclic loading with respect to static moment capacity. This parameter helps in the value of T_b. Graph 4.11a illustrates the effect with variation in ζ_b values while pile geometry is set at l=20m, D=6m and E=1. Normalized accumulated rotation increases with the loading cycle but with a decreasing rate.

Figure 4.11b above shows the effects of the ζ_c parameter on the pile. Length of the pile is 20m, D=6m and E=1. ζ_c is the ratio that tells about the characteristics of the loading cycle where

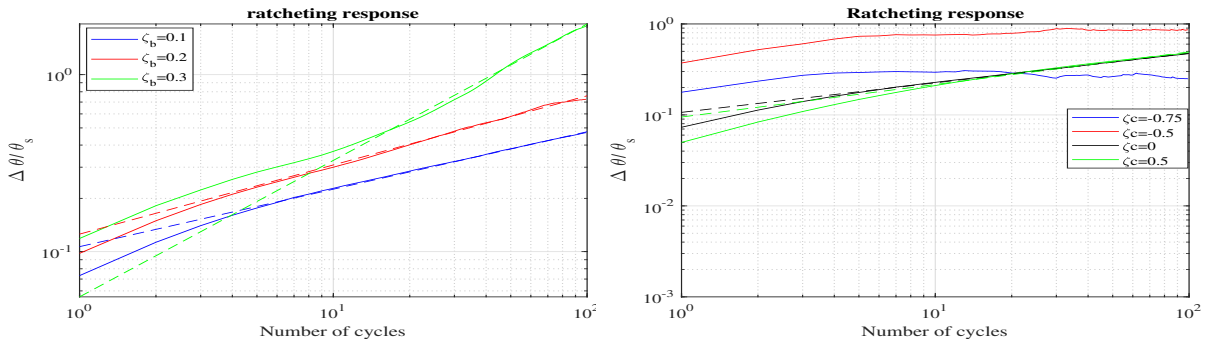

(a) Ratcheting response (ζ_b)

(b) Ratcheting response (ζ_c)

Figure 4.11: Ratcheting response of model under drained cyclic loading while varying (Cyclic Loading factor)

1 means static loading, -1 means two-way loading and 0 equals one-way loading.

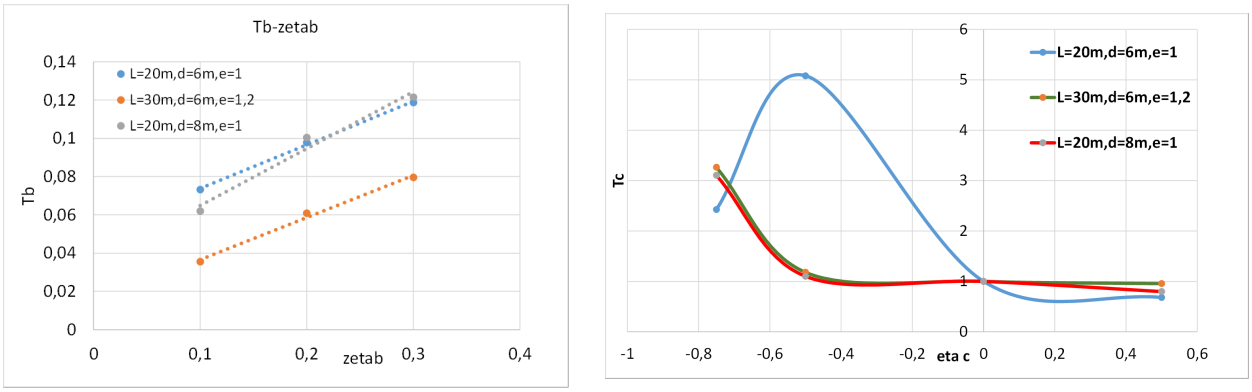

(a) Cyclic dimensionless function (t_b)

(b) Cyclic dimensionless function (t_c)

Figure 4.12: Cyclic dimensionless function

T_b and T_c are the dimensionless functions, that depends directly on load characteristics and relative density. But they can also be formulated through power law equation 4.2. If we compare Equation 2.10 and 4.2 value of A would be directly proportional to the value of T_b and T_c.

$$\frac{\delta\theta(N)}{\theta_0} = AN^b \tag{4.2}$$

$$A(\zeta_c = 0, \zeta_b) = 1 * T_b(\zeta_b) \tag{4.3}$$

T_c equals to 1 for pure one way loading when ζ_c is 0 which is assumed to causes the largest accumulated rotation in the pile. According to [?] value of Tb is a linear line to calculate Tc values . At with $\zeta_c = 1$, T_c value would be 0 because no accumulated displacement under the static loading and also at ζ_c equals to -1, the T_c should be zero since equal and opposite forces are applied. Equation 4.3 shows direct formulation between Tb and Tc. The behaviour of the dimensionless functions T_b is evident with curves easily fitted. The result for the analysis can be seen in figure 4.12 where power law approach is able to capture accumulating rotations for $\zeta_c > 0$. But it can lacks for two way $\zeta_c < 0$ loading, since it captures rotations occurring only in certain number of cycles. From the results it is evident that our assumption earlier about

highest rotation accumulation at $\zeta_c = 0$ was wrong as we can see from figure 4.12b $\zeta_c \leq -0.5$ tends to produce four- five times higher accumulated rotation during cyclic loading.

4.2.4. Visualisation of Cyclic Loading

3D representation of the soil and pile using FEM can be seen from figure 4.13 illustrating changes in the relative density as soil around the pile becomes denser till neutral axis and at the bottom. . Pile1 has been used for the analysis which has length of 20m, diameter of 6m and eccentricity of 1. Bottom and side boundaries are considered fixed. Modelling has been done to study the relative density and strains developed while applying 100 cycles to the stiff monopile.

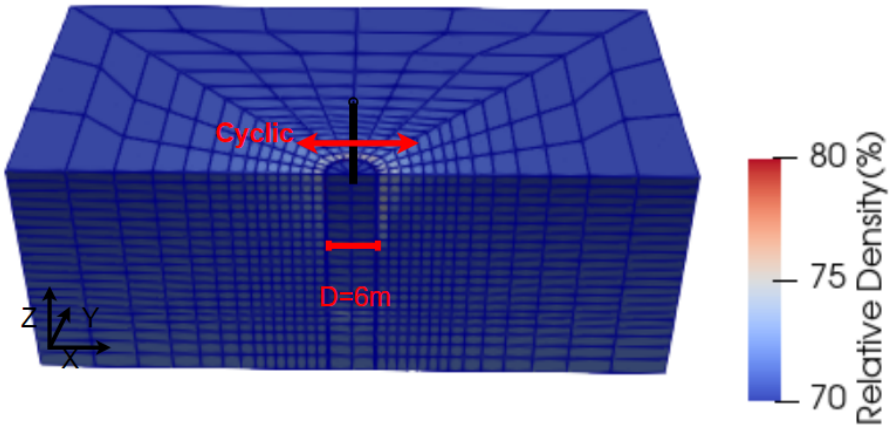

Figure 4.13: Distribution of sand relative density after **100** loading cycles for case **1** in table 4.3

Figure 4.14 presents the magnitude of strains developed around the pile after 100 cycles of loading and unloading. Most of the strains will be developed around the pile top as seen in figure.

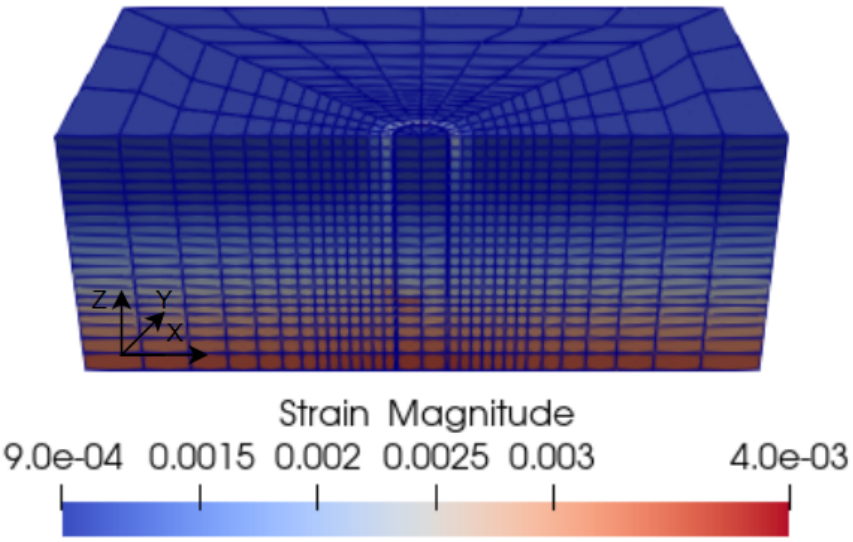

Figure 4.14: Magnitude of strains developed after **100** loading cycles for case **1** in table 4.3

4.2.5. Ratcheting Rates

Figures 4.15a, 4.15b, 4.16 illustrates rotation rates with the help of power law equation. The graphs are drawn between the pile geometry and rotation rates. It can be directly observed from all three graphs that strains tend to remain somewhere between 0.25-0.3 with varying pile geometries.

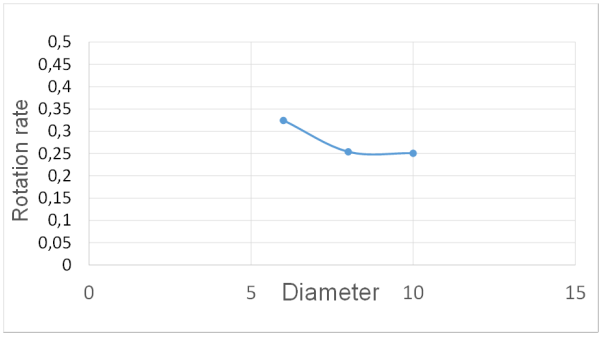

(a) Ratcheting Rate for Diameter

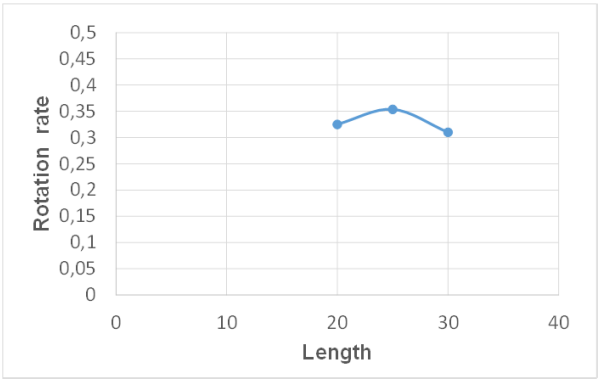

(b) Ratcheting Rate for Length

Figure 4.15: Ratcheting Rate against pile geometry a) Diameter, b) Length

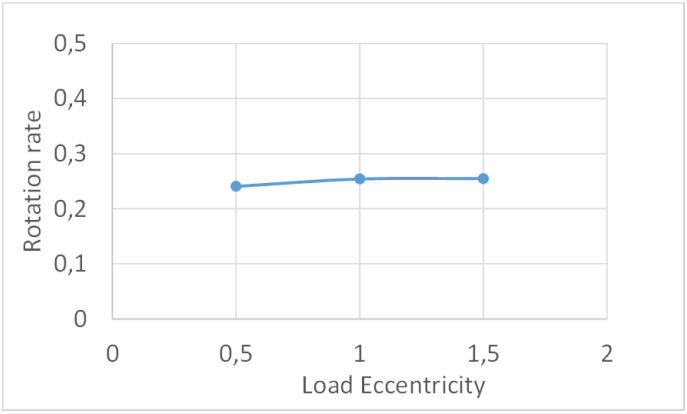

Figure 4.16: Ratcheting Rate against pile geometry Load eccentricity

Figure 4.17a and 4.10b determines the shift in the rotation rate factor (α). For (μ) rate decreases up to 1% and then tend to remain same. And for (ξ) also rotation rates tend to remain same.

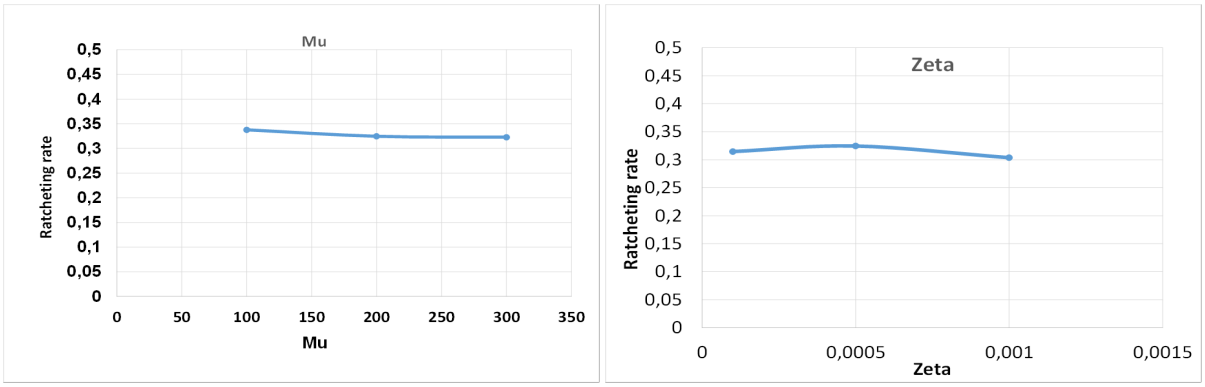

(a) Ratcheting rate (μ)

(b) Ratcheting rate(ξ)

Figure 4.17: Ratcheting rate against (Memory surface parameters) a) (μ), b) (ξ)

Comparing the ratcheting rate (α) for memory surface parameters achieved from SANISAND M.S 3.9and FEM 4.17,it can be concluded that similar behaviour of the graphs is observed. Trends looks identical to each other while the values of alpha factor is different.

4.3. Summary

1. During monotonic loading, pile thickness has no effect on rotation accumulation.
2. Comparing all pile geometry parameters of monopiles (L,E,D), it can be concluded that the most effective solution to decrease the pile rotation due to lateral loading would be to increase the length of the pile.
3. The power law equation can be regarded as an empirical method to predict the pile accumulated rotation. The accumulated rate of monopile rotation are found in range between $0.25 - 0.3$.
4. Increasing magnitude can affect the accumulated rotations in the pile, and this relation ship is linear. This finding does not depend on pile geometry.
5. partial two way loading can induce most dangerous monopile rotation.
6. Memory surface parameters influence the accumulated rotation of monopile, increasing μ value leads to lesser in monopile tilt.

5

Conclusions

5.1. Conclusions :

1. The memory surface parameters in SANISAND-MS model plays vital role in replicating the sand ratcheting behavior during cyclic loading. Parameter μ causes the expansion and contraction of the memory surface due to virgin and non virgin loading. Expansion is corresponded to the compression behaviour of sand and hence higher stiffness, lesser strain accumulation and strengthening of sand. And another parameter analyzed ζ corresponds to the rate with which shrinkage will occur in the memory surface during dilation. So higher value of zeta promotes memory surface contraction and affect sand ratcheting during dilation in terms of strain accumulation and secant stiffness.

2. The SANISAND-MS model was used in the 3D FE modelling of monopile. A series of parameter studies were conducted to study the lateral response of monopile under cyclic loading. Increasing the memory surface parameter μ leads to the higher stiffness of the monopile and the smaller accumulated rotation. This phenomenon is quite similar with the soil element level with SANISAND-MS model in aspect of the decreasing accumulated strain rate with the increasing of load cycles.

3. Sand ratcheting property is natural and instinctive. One can not restrict accumulated rotations during cyclic loading with alliterating pile geometry. Rather it is helpful to study how does these ratcheting property influence the monopile response. Results from the analysis of pile geometry (length, diameter and load eccentricity) suggests that during lateral cyclic loading, with the increase in pile length, rotation accumulation decreases and overall rotation per loading cycle lie between $0.25 - 0.3$ range for all three pile geometry parameters (diameter, length,and load eccentricity).

4. Empirical equation proposed for predicting the long term monopile lateral responses and FE model complement each other upto a certain level. For pure one way cyclic loading, higher amount of rotations are observed with higher magnitude loading. And partial two way loading causes most dangerous monopile.

5.2. Limitations and Recommendations

The conclusions discussed in above section regarding the results obtained through analysing the FEM are quite promising. Still there are some limitation that need to pointed out for the future research work.

1. The SANISAND MS model works effectively for drained triaxial cyclic test whereas for undrained triaxial cyclic test some parameters are needed to be suggested for better performance of the model.
2. Lack of scientific literature and field data restricts SANISAND MS model to be dependent for evaluating strains for 10^6 loading cycles.
3. In order to replicate the actual scenario of pile-soil domain, FEM should take account of the heterogeneity of the soil as well as effects of installations.
4. To validate the FE model, it needs to be calibrated for different soil types and relative densities.

6

Appendix

6.1. Critical surface

r_θ^c indicates the projection of critical state locus on normalized π plane.

$$r_\theta^c = \sqrt{(2/3)}g\theta Mn \tag{6.1}$$

$$n = (r - \alpha)/\sqrt{\frac{2}{3}m} \tag{6.2}$$

g in the equation tells about the shape of the critical locus depending on 'relative' Lode angle θ.

$$G = G_0 p_{atm}[(2.97 - e)^2/(1 + e)]\sqrt{p/p_{atm}} \tag{6.3}$$

$$K = \frac{2}{3}G(\frac{1 + v}{1 - 2v}) \tag{6.4}$$

6.2. Strain superposition

$$R_H = \frac{H_{min}}{H_{max}} \tag{6.5}$$

H_{min},H_{max}states minimum and maximum load applied. β,ϵ,ϕ denotes factors based on soil density, loading method and cyclic loading ratio.

$$t = 0.0032\frac{L}{T}\beta\zeta\phi \tag{6.6}$$

Permanent strains due to 'a' load:

$$\epsilon_{N_a} = \epsilon_{1_a}[1 + t_a \ln(N_a)] \tag{6.7}$$

Permanent strains due to 'b' load:

$$\epsilon_{N_b} = \epsilon_{1_b}[1 + t_b \ln(N_b)] \tag{6.8}$$

After N_b^* cycles with load b, ϵ_{N_b} will be equal to ϵ_{N_a} hence

$$\epsilon_{N_b} = \epsilon_{1_b}[1 + t_b \ln(N_b^*)] \tag{6.9}$$

taking ϵ_{N_b} equals to ϵ_{N_a}

$$N_b^* = \exp \frac{1}{t_b} \frac{\epsilon_{1_a}}{\epsilon_{1_b}} (1 + t_a * \ln(N_a) - 1) \tag{6.10}$$

$$\epsilon_{N_{a+b}} = \epsilon_{1_b}[1 + t_b \ln(N_b + N_b^*)] \tag{6.11}$$

$$y_1 = a_1 (N_1)^{b_1} \tag{6.12}$$

$$a_1 = 0.0002321, b_1 = 0.1785, N_1 = 500, y_1 = 0.000703787$$

$$y_2 = a_2 (N_{12} + N_1)^{b_2} \tag{6.13}$$

$$a_2 = 0.000388, b_2 = 0.1542, N_{12} = 52, y_2 = 0.001027161$$

$$y_3 = a_3 (N_{23} + N_2)^{b_2} + y_2 \tag{6.14}$$

$$a_3 = 0.0005864, b_3 = 0.1359, N_{23} = 67, y_3 = 0.002415214$$

For qd

$$y_1 = a_1 (N_1)^{b_1} \tag{6.15}$$

$$a1 = 0.00121, b1 = 0.2396, N_1 = 500, y_1 = 0.005363627$$

$$y_2 = a_2 (N_{12} + N_1)^{b_2} \tag{6.16}$$

$$a2 = 0.001405, b2 = 0.26, N_{12} = 163, y_2 = 0.007583885$$

$$y_3 = a_3 (N_{23} + N_2)^{b_2} + y_2 \tag{6.17}$$

$$a3 = 0.001561, b3 = 0.3123, N_{23} = 115, y_3 = 0.019181498$$

Bibliography

[1] C. N. Abadie, B. W. Byrne, and G. T. Houlsby. Rigid pile response to cyclic lateral loading: Laboratory tests. Geotechnique, 69(10):863–876, 10 2019.

[2] M. Achmus, J. Albiker, and K. Abdel-Rahman. Investigations on the behavior of large diameter piles under cyclic lateral loading. CRC Press, Boca Raton, FL, USA, 2010.

[3] A. Al-Tabbaa and D. M. Wood. An experimentally basedbubble'model for clay. In International Symposium on Numerical Models in Geomechanics (3rd: 1989)., pages 91–99. Elsevier Applied Science Publishers, 1989.

[4] J. Albiker, M. Achmus, D. Frick, and F. Flindt. 1 g model tests on the displacement accumulation of large-diameter piles under cyclic lateral loading. Geotechnical Testing Journal, 40:173–184, 3 2017.

[5] L. Arany, S. Bhattacharya, J. Macdonald, and S. J. Hogan. Design of monopiles for offshore wind turbines in 10 steps. Soil Dynamics and Earthquake Engineering, 92:126–152, 1 2017.

[6] J. Argyris, G. Faust, J. Szimmat, E. Warnke, and K. Willam. Recent developments in the finite element analysis of prestressed concrete reactor vessels. Nuclear Engineering and Design, 28(1):42–75, 1974. Special Issue: Papers Presented at the Conference.

[7] M. Arshad and B. C. OKelly. Model studies on monopile behavior under long-term repeated lateral loading. International Journal of Geomechanics, 17:04016040, 1 2017.

[8] K. Been and M. Jefferies. Discussion: a state parameter for sands. Géotechnique, 36(1):123–132, 1986.

[9] S. Bhattacharya. Design of foundations for offshore wind turbines. John Wiley & Sons, 2019.

[10] M. Bolton. Discussion: The strength and dilatancy of sands. Géotechnique, 37(2):219–226, 1987.

[11] X. Cheng, A. Diambra, E. Ibraim, H. Liu, and F. Pisanò. 3d fe-informed laboratory soil testing for the design of offshore wind turbine monopiles. Journal of Marine Science and Engineering, 9:1–15, 1 2021.

[12] R. Corti, A. Diambra, D. M. Wood, D. E. Escribano, and D. F. T. Nash. Memory surface hardening model for granular soils under repeated loading conditions. Journal of Engineering Mechanics, 142:04016102, 12 2016.

[13] P. Cuéllar. Pile foundations for offshore wind turbines: numerical and experimental investigations on the behaviour under short-term and long-term cyclic loading. pages 139–195, 2011.

[14] Y. F. Dafalias and M. T. Manzari. Simple plasticity sand model accounting for fabric change effects. Journal of Engineering mechanics, 130(6):622–634, 2004.

[15] M. DeCastro, S. Salvador, M. Gómez-Gesteira, X. Costoya, D. Carvalho, F. Sanz-Larruga, and L. Gimeno. Europe, china and the united states: Three different approaches to the development of offshore wind energy. Renewable and Sustainable Energy Reviews, 109:55–70, 2019.

[16] C. di Prisco and G. Mortara. A multi-mechanism constitutive model for plastic adaption under cyclic loading. International Journal for Numerical and Analytical Methods in Geomechanics, 37(18):3071–3086, 2013.

[17] D. Frick and M. Achmus. An experimental study on the parameters affecting the cyclic lateral response of monopiles for offshore wind turbines in sand. Soils and Foundations, 60:1570–1587, 12 2020.

[18] V. N. Georgiannou, A. Tsomokos, and K. Stavrou. Monotonie and cyclic behaviour of sand under torsional loading. Geotechnique, 58:113–124, 3 2008.

[19] Y. T. Huang, A. B. Huang, Y. C. Kuo, and M. D. Tsai. A laboratory study on the undrained strength of a silty sand from central western taiwan. Soil Dynamics and Earthquake Engineering, 24:733–743, 10 2004.

[20] H. Jostad, G. Grimstad, K. Andersen, M. Saue, Y. Shin, and D. You. A fe procedure for foundation design of offshore structures–applied to study a potential owt monopile foundation in the korean western sea. Geotechnical Engineering Journal of the SEAGS & AGSSEA, 45(4):63–72, 2014.

[21] M. E. Kalinski. Soil mechanics: lab manual. Number Ed. 2. John Wiley & Sons, 2011.

[22] D. Kallehave, C. L. Thilsted, and M. Liingaard. Modification of the api py formulation of initial stiffness of sand. In Offshore site investigation and geotechnics: integrated technologies-present and future, pages 465–472. OnePetro, 2012.

[23] R. Kelly, G. Houlsby, and B. Byrne. A comparison of field and laboratory tests of caisson foundations in sand and clay. Géotechnique, 56(9):617–626, 2006.

[24] E. Kementzetzidis, S. Corciulo, W. G. Versteijlen, and F. Pisanò. Geotechnical aspects of offshore wind turbine dynamics from 3d non-linear soil-structure simulations. Soil Dynamics and Earthquake Engineering, 120:181–199, 2019.

[25] E. Kementzetzidis, W. G. Versteijlen, A. Nernheim, and F. Pisano. 3d fe dynamic modelling of offshore wind turbines in sand: natural frequency evolution in the pre–to after-storm transition. Numerical methods in geotechnical engineering IX, 2:1477–1484, 2018.

[26] R. T. Klinkvort and O. Hededal. Lateral response of monopile supporting an offshore wind turbine. Proceedings of the Institution of Civil Engineers-Geotechnical Engineering, 166(2):147–158, 2013.

[27] C. Leblanc, B. W. Byrne, and G. T. Houlsby. Response of stiff piles to random two-way lateral loading. Geotechnique, 60:715–721, 2010.

[28] C. LeBlanc, G. T. Houlsby, and B. W. Byrne. Response of stiff piles in sand to long-term cyclic lateral loading. Geotechnique, 60:79–90, 2 2010.

[29] S.-S. Lin and J.-C. Liao. Permanent strains of piles in sand due to cyclic lateral loads. Journal of geotechnical and geoenvironmental engineering, 125(9):798–802, 1999.

[30] H. Liu, J. Abell, A. Diambra, and F. Pisano. Capturing cyclic mobility and preloading effects in sand using a memory-surface hardening model. In Proc. of 7th Int. Conf. on Earthquake Geotechnical Engineering (7ICEGE), pages 17–20, 2019.

[31] H. Y. Liu, J. A. Abell, A. Diambra, and F. Pisanò. Modelling the cyclic ratcheting of sands through memory-enhanced bounding surface plasticity. Geotechnique, 69(9):783–800, 9 2019.

[32] H. Y. Liu and F. Pisanò. Prediction of oedometer terminal densities through a memory-enhanced cyclic model for sand. Geotechnique Letters, 9(2), 6 2019.

[33] J. Long and G. Vanneste. Effects of cyclic lateral loads on piles in sand. Journal of Geotechnical Engineering, 120(1):225–244, 1994.

[34] M. T. Manzari and Y. F. Dafalias. A critical state two-surface plasticity model for sands. Geotechnique, 47(2):255–272, 1997.

[35] Z. Mrz, V. Norris, and O. Zienkiewicz. An anisotropic hardening model for soils and its application to cyclic loading. International Journal for Numerical and Analytical Methods in Geomechanics, 2(3):203–221, 1978.

[36] M. U. Østergaard, A. H. Augustesen, S. P. H. Sørensen, C. Kramhøft, and M. T. Larsen. Modelling of soil-pile interaction for monopiles for offshore wind turbines: Back-calculation of eigenfrequencies. In Vietnam Symposium on Advances in Offshore Engineering, pages 190–195. Springer, 2018.

[37] A. G. Papadimitriou and G. D. Bouckovalas. Plasticity model for sand under small and large cyclic strains: a multiaxial formulation. Soil Dynamics and Earthquake Engineering, 22(3):191–204, 2002.

[38] A. G. Papadimitriou, G. D. Bouckovalas, and Y. F. Dafalias. Plasticity model for sand under small and large cyclic strains. Journal of geotechnical and geoenvironmental engineering, 127(11):973–983, 2001.

[39] J. Park and J. C. Santamarina. Sand response to a large number of loading cycles under zero-lateral-strain conditions: Evolution of void ratio and small-strain stiffness. Geotechnique, 69:501–513, 6 2019.

[40] I. Pineda. Offshore wind in europe windeurope business intelligence tom remy (construction highlights) ariola mbistrova (financing highlights) courtesy of Øyvind gravås statoil-floating offshore wind farm: Hywind scotland, 2018.

[41] T. J. Price. James blythbritain's first modern wind power pioneer. Wind engineering, 29(3):191–200, 2005.

[42] I. A. Richards, B. W. Byrne, and G. T. Houlsby. Monopile rotation under complex cyclic lateral loading in sand. Geotechnique, 70:916–930, 10 2020.

[43] A. Shonberg, M. Harte, A. Aghakouchak, C. Brown, M. P. Andrade, and M. Liingaard. Suction bucket jackets for offshore wind turbines: applications from in situ observations. In Proc. TC209 Workshop, 19th International Conference on Soil Mechanics and Geotechnical Engineering, Seoul, South Korea, pages p65–77, 2017.

[44] P. Staubach and T. Wichtmann. Long-term deformations of monopile foundations for offshore wind turbines studied with a high-cycle accumulation model. Computers and Geotechnics, 124:103553, 2020.

[45] P. Truong, B. M. Lehane, V. Zania, and R. T. Klinkvort. Empirical approach based on centrifuge testing for cyclic deformations of laterally loaded piles in sand. Geotechnique, 69:133–145, 2 2019.

[46] T. Wichtmann. Soil behaviour under cyclic loadingexperimental observations, constitutive description and applications. habilitation. Karlsruhe Institute for Technology KIT, Institute of Soil Mechanics and Rock Mechanics IBF. Heft, (81), 2016.

[47] D. Wijewickreme and M. Sanin. Cyclic shear loading response of fraser river delta silt. In Proceedings of the 13th world conference on earthquake engineering, Vancouver, BC, pages 1–6, 2004.

[48] D. Wijewickreme, M. V. Sanin, and G. R. Greenaway. Cyclic shear response of fine-grained mine tailings. Canadian Geotechnical Journal, 42(5):1408–1421, 2005.